Research Division
NATIONAL RESEARCH CORPORATION
70 Memorial Drive
Cambridge, Massachusetts 02142

NRC Project No. 86-1-0609

SUMMARY REPORT

CONTRACT NASw - 962

STUDY OF THE MECHANISM OF ATMOSPHERIC INTERACTION WITH THE FATIGUE OF METALS

July 1, 1964 to August 3, 1965

by

M. J. Hordon
M. E. Reed

Approved by: Norman Beecher
Norman Beecher
Assistant Director of Research

Reviewed by: Frank J. Salomone
Frank J. Salomone
Contracts Manager

Submitted to:

Headquarters
National Aeronautics and Space Administration
400 Maryland Avenue
Washington, D. C.
ATTENTION:
Director of Space Research and Technology
Office of Advanced Research and Technology
Code RRM

TABLE OF CONTENTS

LIST OF FIGURES

LIST OF TABLES

SUMMARY

Measurements of the fatigue behavior of 1100 aluminum in vacuum environments have shown that a substantial increase in fatigue resistance occurred at all stress levels. The increase in fracture life, compared to similar tests in air, was attributed to a decrease in the crack propagation rate in the absence of oxygen or water vapor gas. A transition pressure of 10^{-2} - 10^{-3} torr was observed below which crack retardation was marked. The critical pressure was attributed to the effect of molecular adsorption rates on crack growth. The crack growth rate was found to be dependent on the cyclic stress frequency as well as pressure level in accordance with the adsorption mechanism.

In Phase II of the program, design and construction of a unique fatigue apparatus for extremely high vacuum conditions was initiated. The apparatus will test up to eight specimens simultaneously at fixed strain amplitudes in vacuums below 10^{-12} torr utilizing the XHV (Extreme High Vacuum) system developed at National Research Corporation. Preliminary tests in air have shown that cyclic rates up to 200 cps will be feasible in the vacuum unit.

1.0 FOREWORD

This is the Summary Report covering work performed in the Research Division of National Research Corporation under Contract No. NASw-962 for the Office of Advanced Research and Technology, National Aeronautics and Space Administration during the period July 1, 1964, to August 3, 1965.

The object of this investigation was to examine the fatigue behavior of a representative structural material as a function of applied stress, cyclic frequency and vacuum level. The comparison of fatigue properties at reduced pressures down to 10^{-12} torr and at atmosphere would be expected to provide an insight to the mechanisms of surface atmospheric interaction with fatigue crack nucleation and growth process.

The program was divided into two major phases: Phase I, investigation of fatigue properties in pressure range 7.6×10^{2} (unit atmosphere) to 10^{-7} torr; and Phase II, supplementary investigations at vacuum levels up to 10^{-12} torr using the Extreme High Vacuum (XHV) facilities developed at National Research Corporation.

Major contributors to this program were Dr. M. J. Hordon, Dr. J. L. Ham and M. E. Reed of the research staff of NRC and Professor G. S. Reichenbach of Massachusetts Institute of Technology.

Some of the results of this work were presented at the Sixth Annual Symposium on Space Environmental Simulation, May, 1964.[1]

2.0 INTRODUCTION

Interest in the effect of outer space environments on the physical and mechanical properties of engineering materials has substantially increased in recent years with the growing pace of our satellite and lunar research effort. The need for more precise and extensive information on the extra terrestrial behavior of materials has developed in proportion to the expanding reliability requirements as more complex vehicles probe deeper into space for longer periods of time.

With respect to materials properties in space, the high vacuum level, estimated at 10^{-12} torr above 2000 km height[2] is of major interest. The relative absence of oxygen or water vapor molecules to react with metal surfaces as well as the likely degredation of existing adsorbed films by mechanical abrasion or cosmic erosion will strongly influence surface-sensitive properties such as fatigue.

The influence of low pressure environment on the fatigue properties of metals and alloys has been well established since the initial work of Gough and Sopwith in 1932.[3] Several investigations [4-7] have shown that the fatigue resistance of a variety of materials including copper, aluminum, carbon steel, and stainless steel improved substantially with pressures below 10^{-3} torr. The increase in fatigue life ranged from 2 to 60 fold depending on the applied stress, type of material, vacuum level

and the residual gas content. Generally, a much greater degree of surface roughening or slip extrusion-intrusion steps were observed in vacuum tested specimens which could be attributed to an increase in planar slip in the absence of barrier oxide films.

Prior investigations by Ham and Reichenbach[8] have shown the presence of a critical pressure range affecting fatigue behavior in aluminum. A substantial increase in fatigue life compared to atmosphere was observed in the vacuum range 10^{-2} to 10^{-4} torr. Further increase in vacuum level produced relatively little enhancement of the fracture life. It has been suggested that these results reflect a critical pressure dependence of mono-layer oxygen or hydrogen ion adsorption at the fatigue crack surfaces.

3.0 PHASE I

3.1 Introduction

In order to examine in greater detail the important effects on fatigue properties at moderate vacuum levels, the initial phase of the program was designed to investigate in the vacuum range extending from unit atmosphere to 10^{-7} torr. A multi-station fatigue testing unit was designed and constructed to test up to eight samples simultaneously at the same vacuum level.

The fatigue properties of 1100 aluminum in reverse bending were determined at four constant strain amplitude levels and two cyclic frequencies. During the tests, measurements were taken of the number of cycles to initiate the fracture crack and the rate of crack growth. For selected samples, measurements were also taken of the moment force, corresponding to the change in fatigue stress with cyclic life.

3.2 Apparatus

The apparatus used in the Phase I studies and hereafter denoted as Unit I consists of a massive circular flange plate 27.5 in. in diameter. Mounted under the flange plate, as shown in Fig. 1, is an octogonal base plate which acts as a fixed central base for the eight radially positioned samples. Four of the base plate projections, Stations 1, 2, 5 and 6 are furnished with electrical resistance strain gage assemblies to determine the flexure of the specimens through the related motion of the base plate projections.

The outer ends of the specimens are fastened to crank rods through flexible spring steel connectors which absorb the eccentricity of the rod motion. The rods are carried through the flange plate by means of bellows seals capable of $\pm$ 0.10 in. motion with design cyclic lifetime above 10^8 oscillations.

As shown in Fig. 2, the crank rods are bolted to eccentric bearing assemblies in turn connected to 1/15 H.P. motors concentrically positioned on the flange plate. To vary the vertical thrust of the rod and, hence, the bending moment of the sample, complete eccentric units varying from 0.025 to 0.040 in. can be installed in the bearing housing. The motor drives for each station are individually controlled allowing a range of bending frequencies varying from 2 to 53 cps. Each station is provided with a glass viewing port, a control relay stop switch and a cycle counter connected to the motor drive.

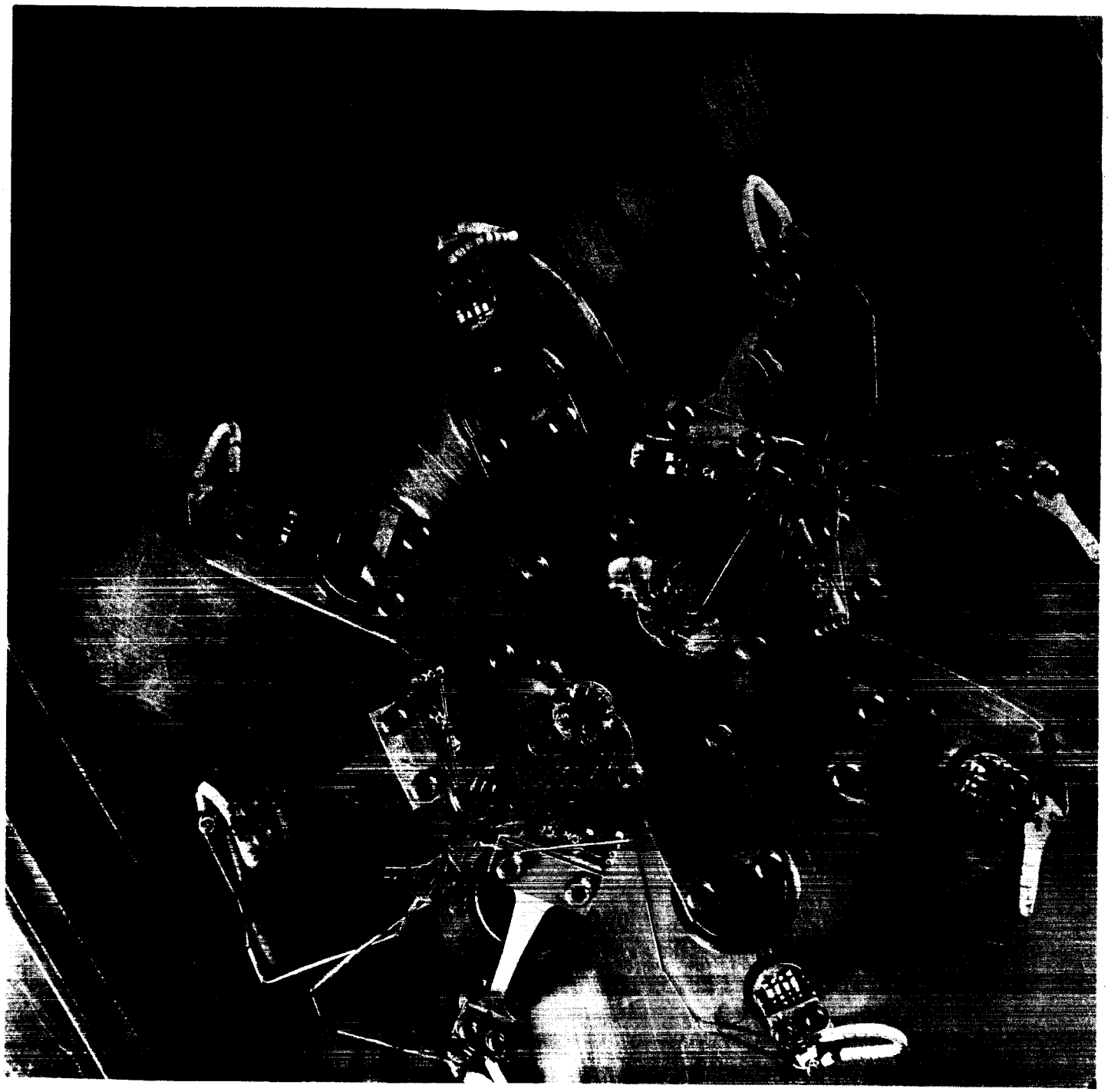

FIGURE 1

Bottom View of Vacuum Fatigue Base Flange Unit

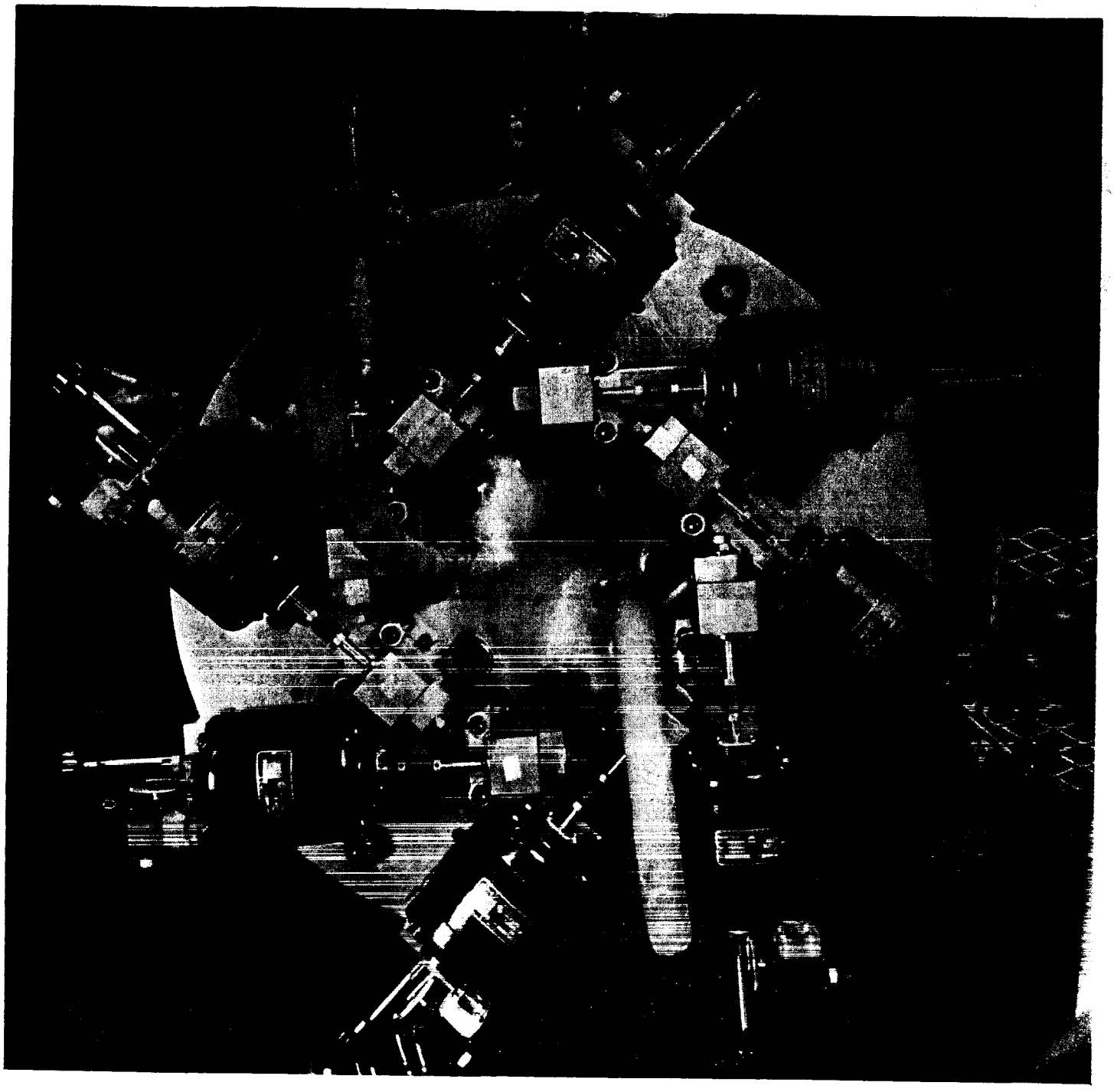

FIGURE 2

Top View of Vacuum Fatigue Apparatus

The flange and base plate assembly and a cylindrical component which forms the body of the vacuum chamber are coupled to a standard Varian Vac Ion unit. The entire assembly is shown in Fig. 3. The unit can provide a vacuum of 2×10^{-7} torr with all eight specimens without thermal outgassing. The Vac Ion pump has the great advantage of avoiding the use of diffusion pump oil, thus eliminating the possibility of hydrocarbon contamination during long fatigue tests.

For use in the fatigue testing unit, a fixed end cantilever - type specimen was selected with the dimensions shown in Fig. 4. The specimen geometry was closely similar to the standard ASTM design for constant stress along the gage length. With the aluminum samples used in the present investigation (1100-H14 Al, BHN = 32), a design thickness of 0.185 in. required a force of about 20 lbs. to achieve the maximum bending amplitude of 0.040 in. The strain amplitudes in reversed bending were chosen to produce fatigue fractures in the range 5×10^4 to 10^7 cycles.

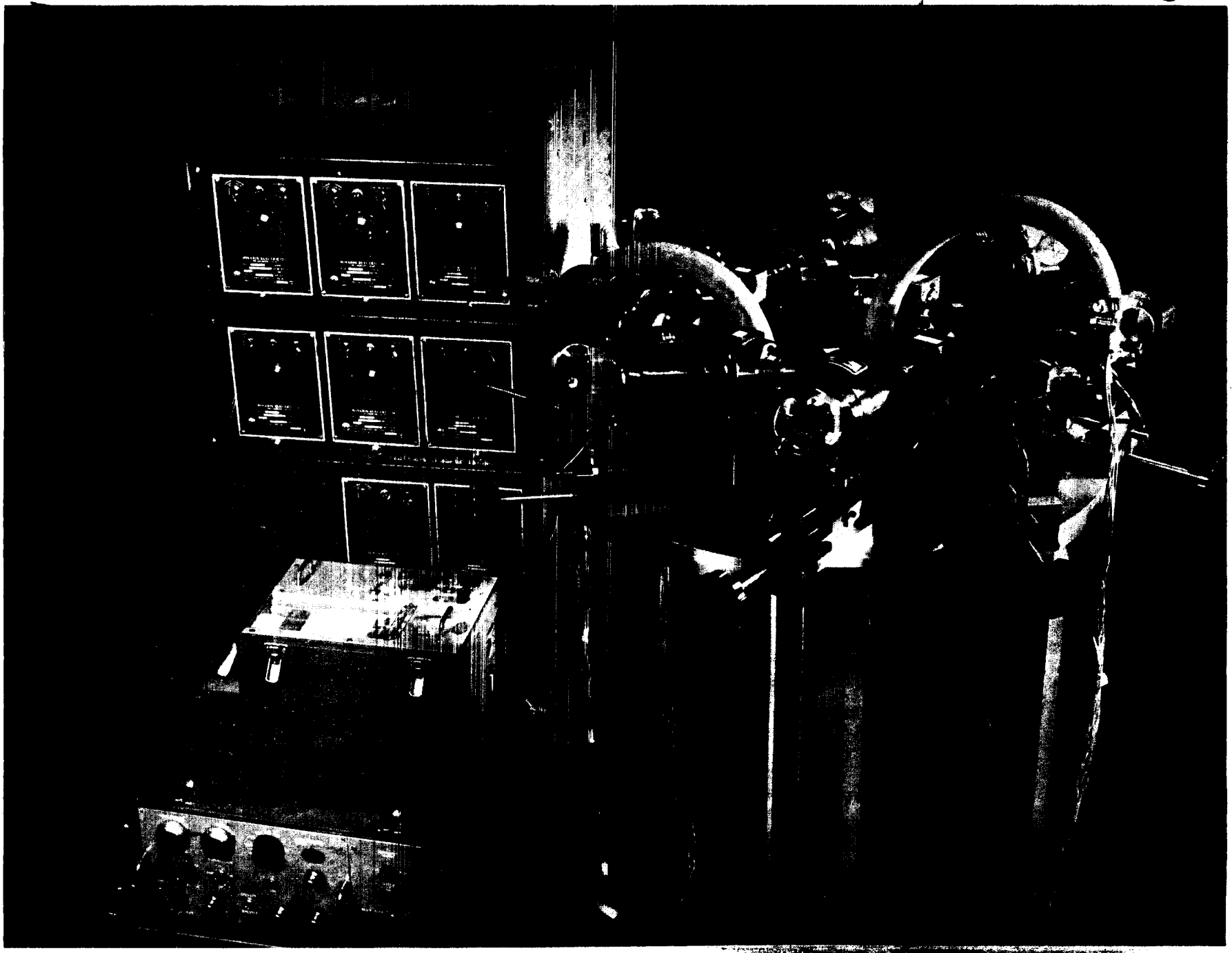

FIGURE 3 Vacuum Fatigue Testing Unit with Control Panel

SPECIMEN OUTLINE

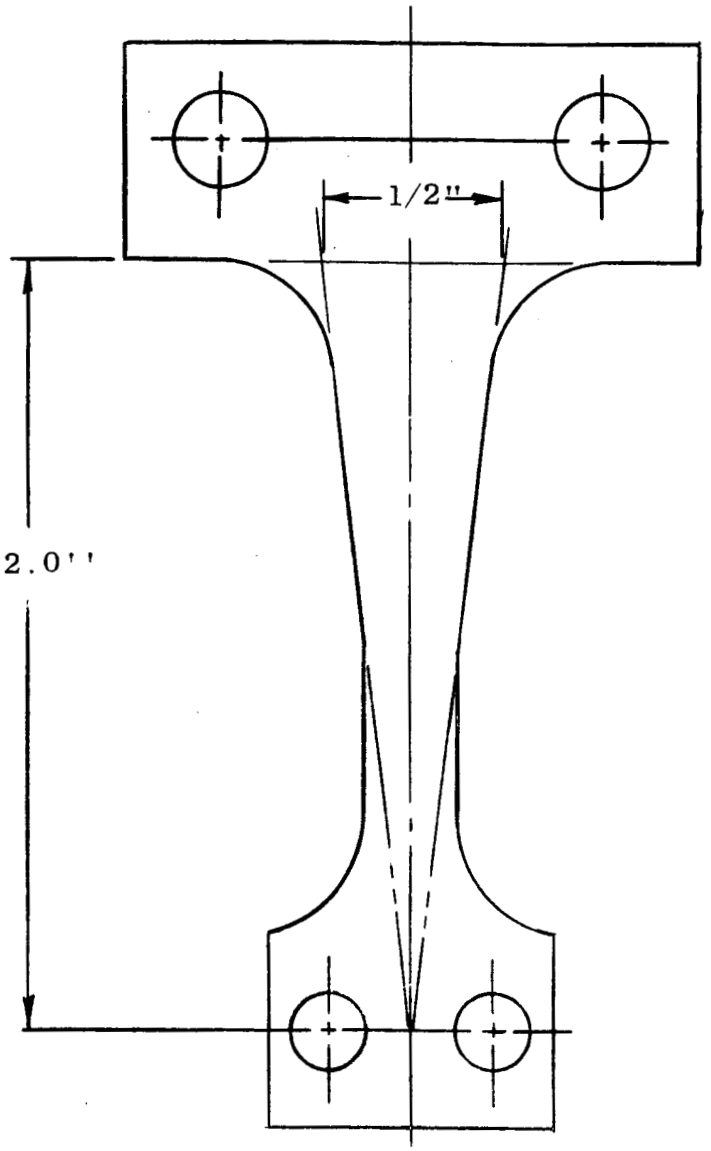

FIGURE 4

3.3 Test Procedure

Fatigue test specimens were carefully machined from 1100 - H14 aluminum sheet stock. After final grinding, the gage section surfaces were polished on successively finer lapping paper until a smooth, nick-free contour was obtained. Dimensional tolerances for all specimens were held to $\pm$ 0.002 in. in width and $\pm$ 0.001 in. in thickness.

Fatigue tests were run at selected vacuum levels according to the following procedures:

1. Specimens were selected at random and checked for dimensions.

2. After pumpdown to a stable vacuum, simultaneous fatigue tests were run at cyclic frequencies of 25 and 50 cps.

3. For each constant strain amplitude and vacuum level, four stations each were operated at the two frequencies. The stations were alternated in successive pumpdowns to average the results of individual amplitudes.

4. Eight individual tests were run for each strain amplitude and frequency to obtain a high degree of confidence in the fatigue life data.

5. Additional tests were performed if excessive deviations were observed in the data.

6. During the fatigue tests, visual observations of crack formation and growth were recorded as a function of the cyclic life.

Selected samples were monitored for moment force measurements using a recorder to indicate changes in specimen stress level.

7. The total fatigue life was taken as 100 pct crack extension across the sample gage section.

3.4 RESULTS

Pressure Dependence of the Fatigue S-N Curve

Measurements of the fracture life in reverse bending fatigue for 1100-H14 aluminum were conducted at constant strain amplitudes in the range 0.001 to 0.002 corresponding to maximum tensile and bend stresses in the range 8,000 to 14,000 psi. The tests were made at pressure levels varying from 1×10^{-7} to 1×10^{-3} torr and were compared with equivalent atmospheric data. The fatigue tests were run at two constant bending rates of 25 and 50 cps.

Comparative fatigue data in the form of fatigue stress vs. cyclic life plots (S-N curves) are shown in Fig. 5 for 2×10^{-7} torr and unit atmosphere (7.6×10^{2} torr). The experimental points comprise the mean value for a minimum of five experimental tests, in most cases, eight tests were made for each pressure, frequency and stress condition.

It is evident that the evacuation of air resulted in a substantial increase in total fatigue life. Particularly for the lower stress levels, the fatigue improvement factor was as high as ten-fold. Doubling the cyclic frequency, however, resulted in only a 75 pct enhancement of the fracture life.

The S-N curve comparative data for pressure levels of 1×10^{-5} and 1×10^{-3} torr are shown in Figs. 6 and 7. Substantial increases in fatigue resistance were noted similar to the results obtained at lower pressure.

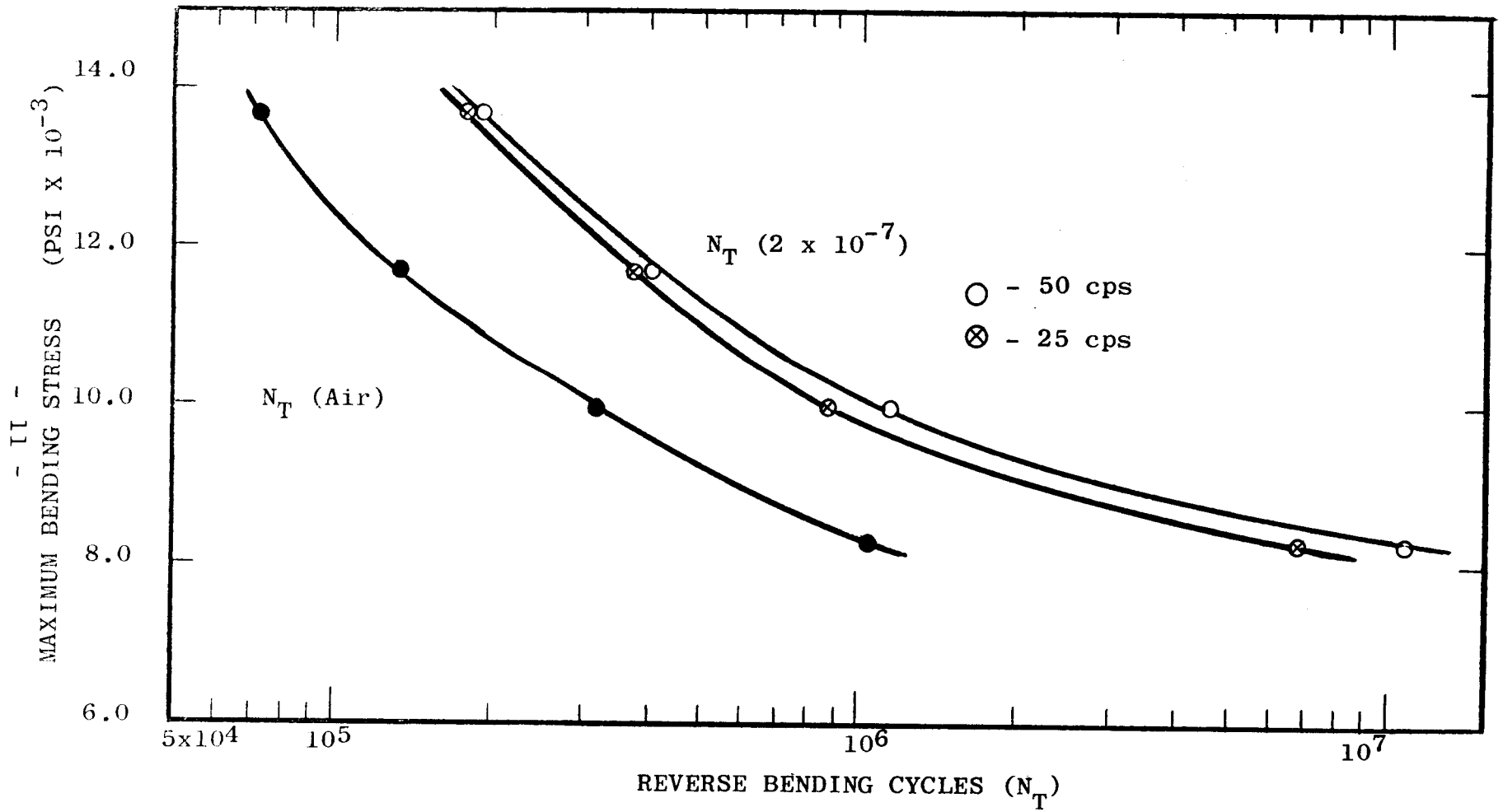

COMPARISON OF THE TOTAL FRACTURE LIFE N_T WITH MAXIMUM BENDING STRESS AT 2×10^{-7} TORR VACUUM AND AT ATMOSPHERE.

FIGURE 5

FIGURE 6

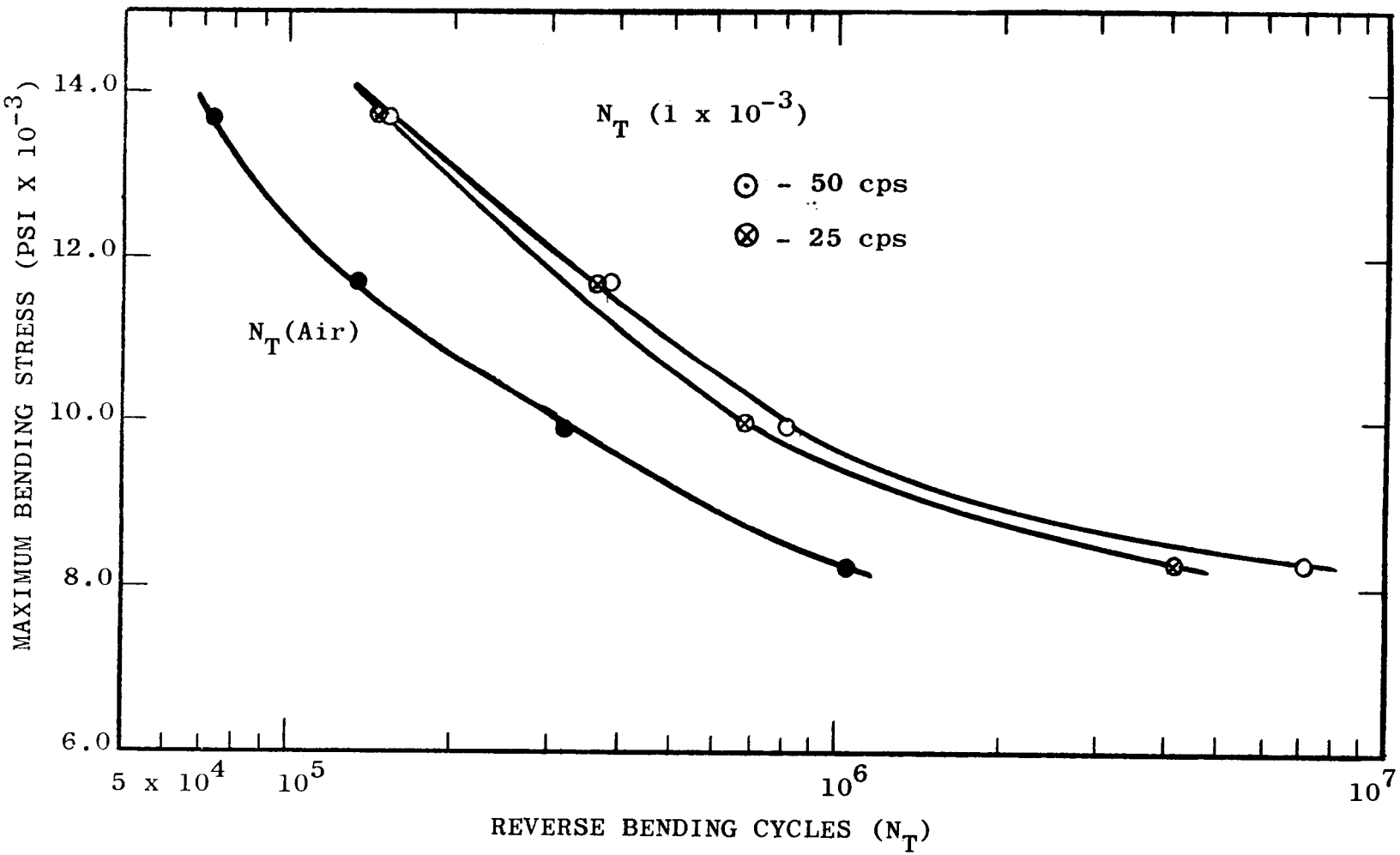

COMPARISON OF THE TOTAL FRACTURE LIFE N_T WITH MAXIMUM BENDING STRESS AT 10^{-3} TORR VACUUM AND AT ATMOSPHERE.

FIGURE 7

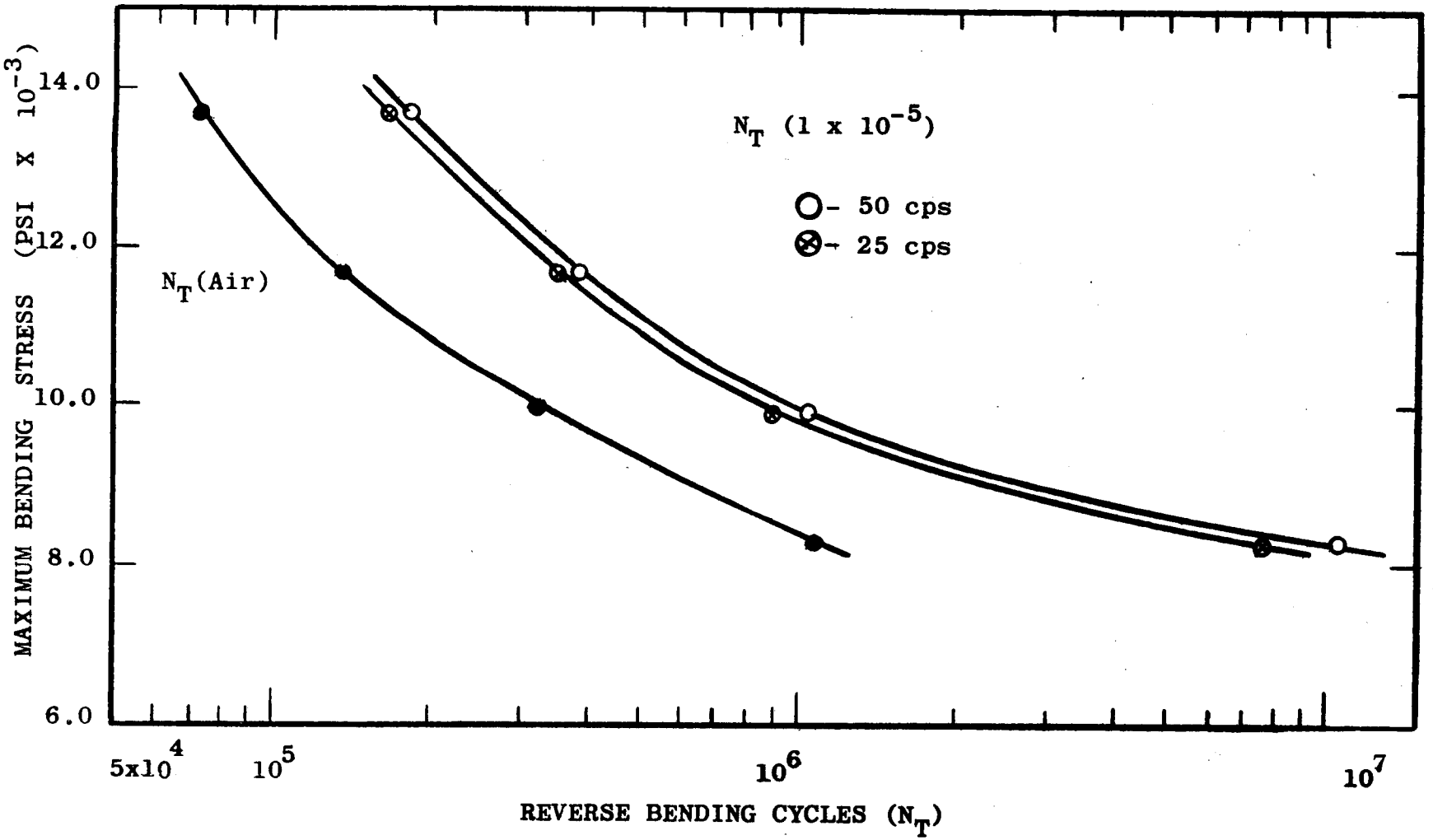

COMPARISON OF THE TOTAL FRACTURE LIFE N_T WITH MAXIMUM BENDING STRESS AT 10^{-5} TORR VACUUM AND AT ATMOSPHERE.

The composite pressure dependence of the fatigue behavior of 1100 aluminum can be represented by a P-N curve similar to the standard S-N plots. Fig. 8 shows the variation of fracture life with pressure at four constant strain amplitudes as a function of cyclic rate. Additional fatigue data for the lowest strain value, $\varepsilon = 0.0012$ ($\sigma_{max.} = 8{,}300$ psi), were taken at the intermediate pressure levels of 0.1 and 0.01 torr in order to complete the P-N curve.

The P-N plots show that there is a major step in fatigue resistance at approximately 10^{-2} torr. The discontinuity is found at all strain levels and frequencies examined. At pressures above 0.01 torr, the fracture life was only slightly increased above the standard atmospheric value. At pressures below 10^{-4} torr, the fatigue enhancement remained relatively stable. Further reduction of pressure below 10^{-5} torr resulted in a diminishing rate of fatigue improvement.

Pressure Dependence Of Crack Nucleation

The fatigue process can generally be separated into two major components: Stage 1, comprising that portion of the fracture life required to nucleate or initiate a dominant crack, and Stage 2, the number of stress cycles to propagate the crack through the specimen to final fracture. Recently, it has been proposed that the crack through the specimen to final fracture. Recently, it has been proposed that the crack propagation phase itself may be

FIGURE 8

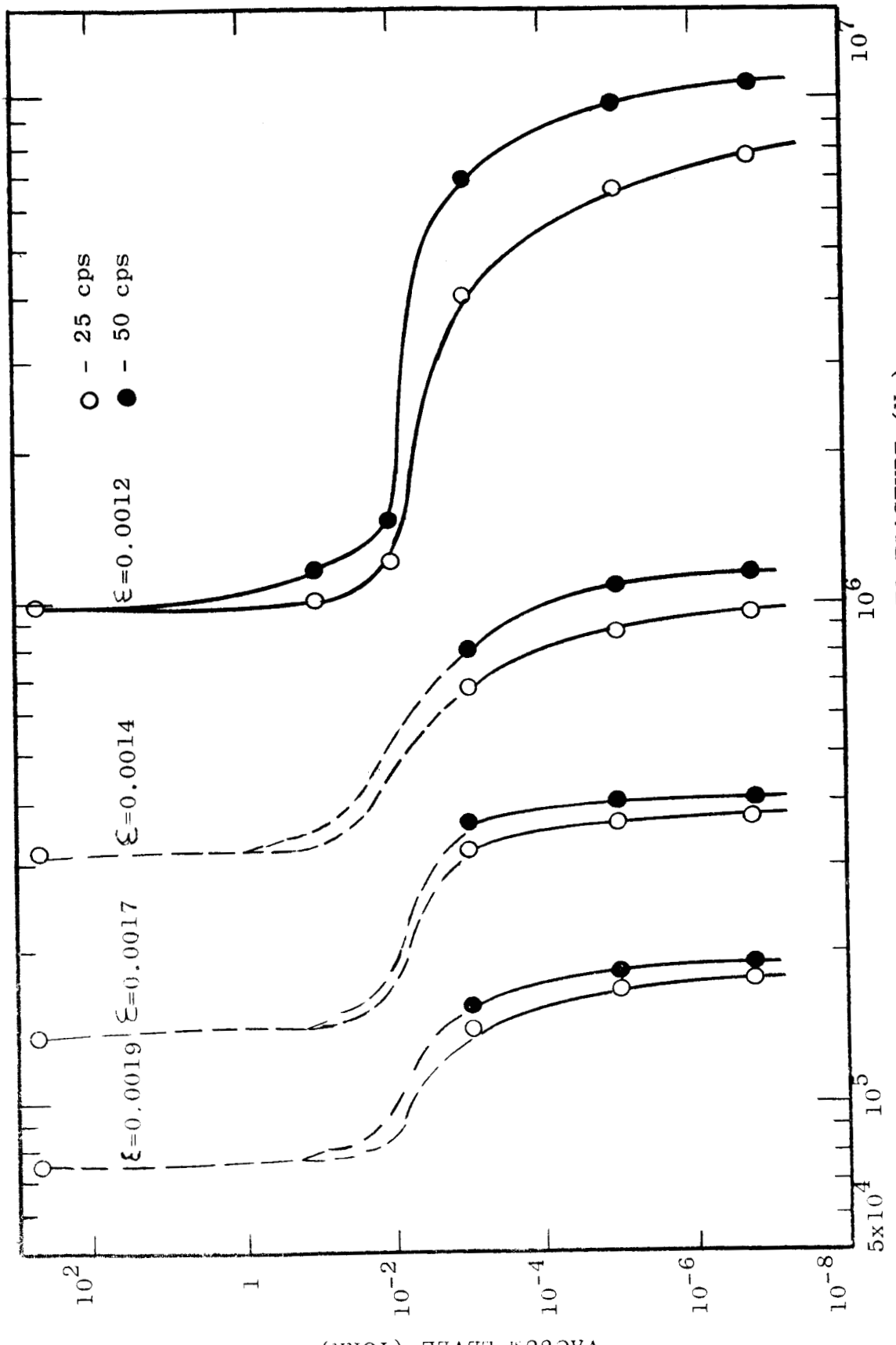

PRESSURE DEPENDENCY OF THE FATIGUE LIFE OF ALUMINUM WITH STRAIN AMPLITUDE AND CYCLIC FREQUENCY.

divided into two substages, the initial portion consisting of the slow growth of individual microcracks followed by the more rapid catastrophic propagation of a macrocrack in the terminal phase. [9] The fatigue behavior may then be denoted:

$$N_T = N_I + (N^1_P + N_P) \qquad (1)$$

where N_T is the total fracture life, N_I is the number of cycles to nucleate microcracks, N^1_P is the number of cycles required to enlarge the microcracks to the critical growth size and N_P and is the number of cycles required to propagate the dominant crack across the specimen.

In the current investigation, optical measurements of crack formation and subsequent growth were made during fatigue tests. The minimum detectable crack length under testing conditions was about 10^{-2} cm. Hence, the experimental nucleation phase included $(N_I + N^1_P)$. In the N_P phase, measurements of the crack propagation rate were made as a function of stress, pressure and cyclic frequency.

The variation of the experimental nucleation stage with fatigue stress as a function of vacuum level and cycle rate is shown in Fig. 9. It is evident that the number of fatigue cycles to initiate a measureable crack was only slightly sensitive to the vacuum environment. The small increase in fatigue resistance may be attributed to the dependence of N^1_p on the surface gas density. It is apparent that fatigue crack nucleation was relatively insensitive to the surface vacuum environment, indicating that crack formation was largely an internal process.

Pressure Dependence of Crack Propagation

Fig. 10 presents the P-N_p family of curves after subtracting the initial stage from the fracture life. Comparison with Fig. 8 shows that the fracture retardation in vacuum appeared to be the mechanism controlling fatigue behavior in aluminum.

The influence of surface vacuum environment on the rate of crack growth under repeated loading is indicated in Fig. 11 for the series of fatigue tests at the constant strain of 0.0012 (σ = 8,300 psi) and 50 cps bending frequency. The average major crack was first detected under these conditions after about 2×10^5 cycles in air. Fracture occurred at less than 9×10^5 cycles requiring approximately 13,000 sec for extension of the crack across the specimen. Under vacuum conditions, the time required for crack propagation increased substantially reaching a maximum of 240,000 sec at 2×10^{-7} torr, corresponding to a propagation life of about 11×10^6 cycles. As

FIGURE 9

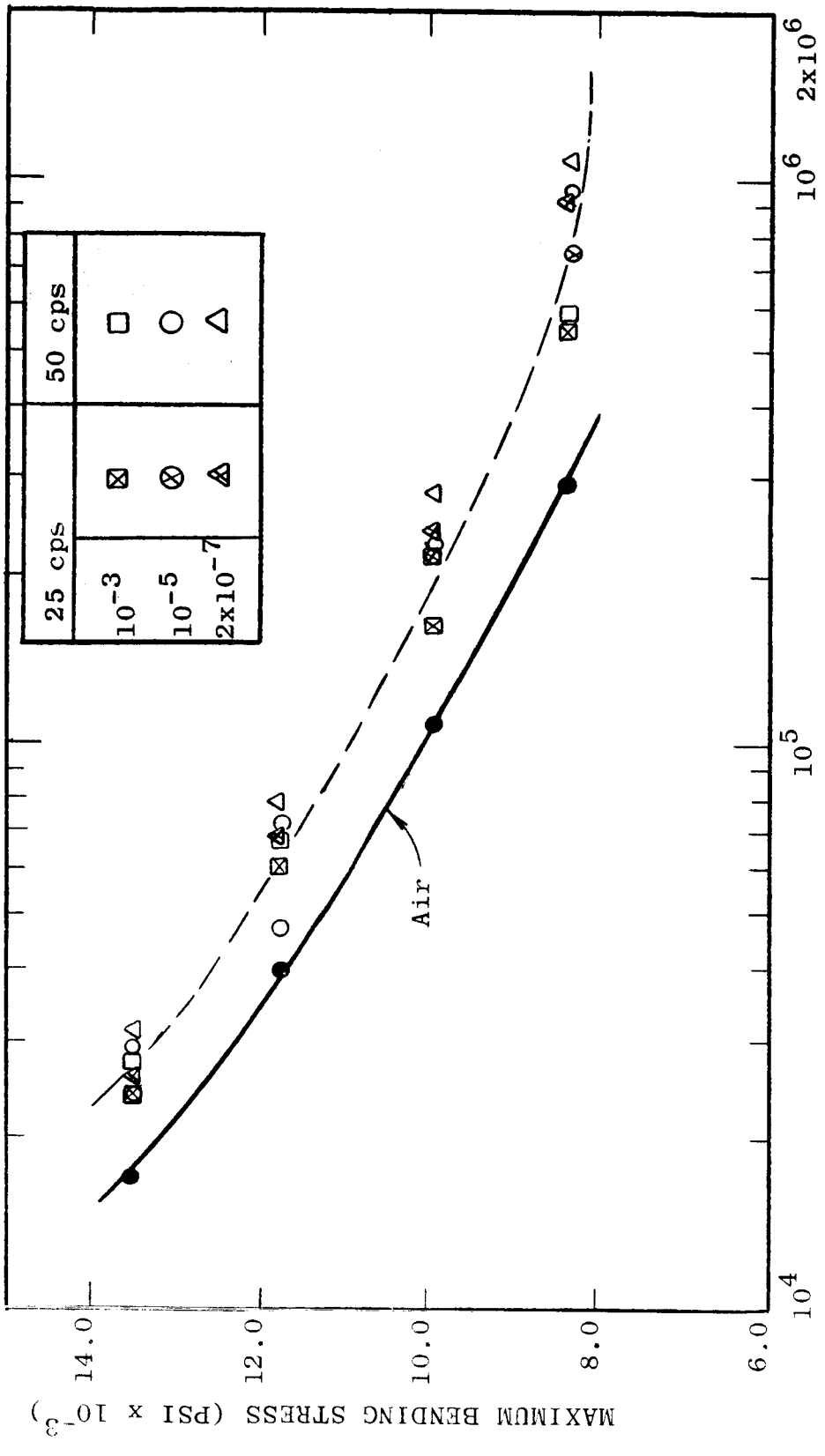

VARIATION OF THE CRACK NUCLEATION LIFE N_I WITH MAXIMUM BENDING STRESS IN VACUUM AND IN ATMOSPHERE.

FIGURE 10

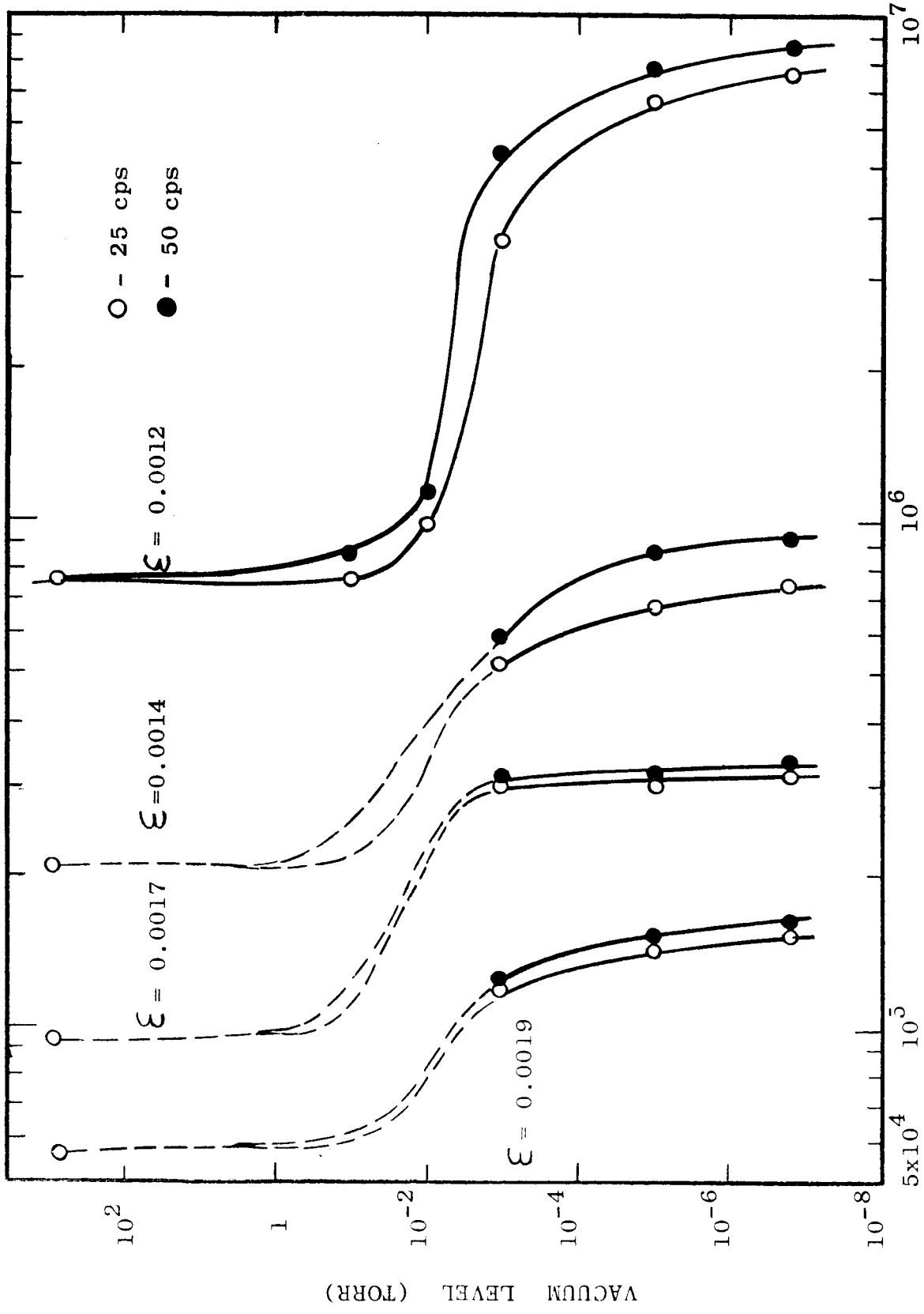

PRESSURE DEPENDENCE OF THE CRACK PROPAGATION LIFE N_p OF ALUMINUM WITH STRAIN AMPLITUDE AND CYCLIC FREQUENCY.

FIGURE 11

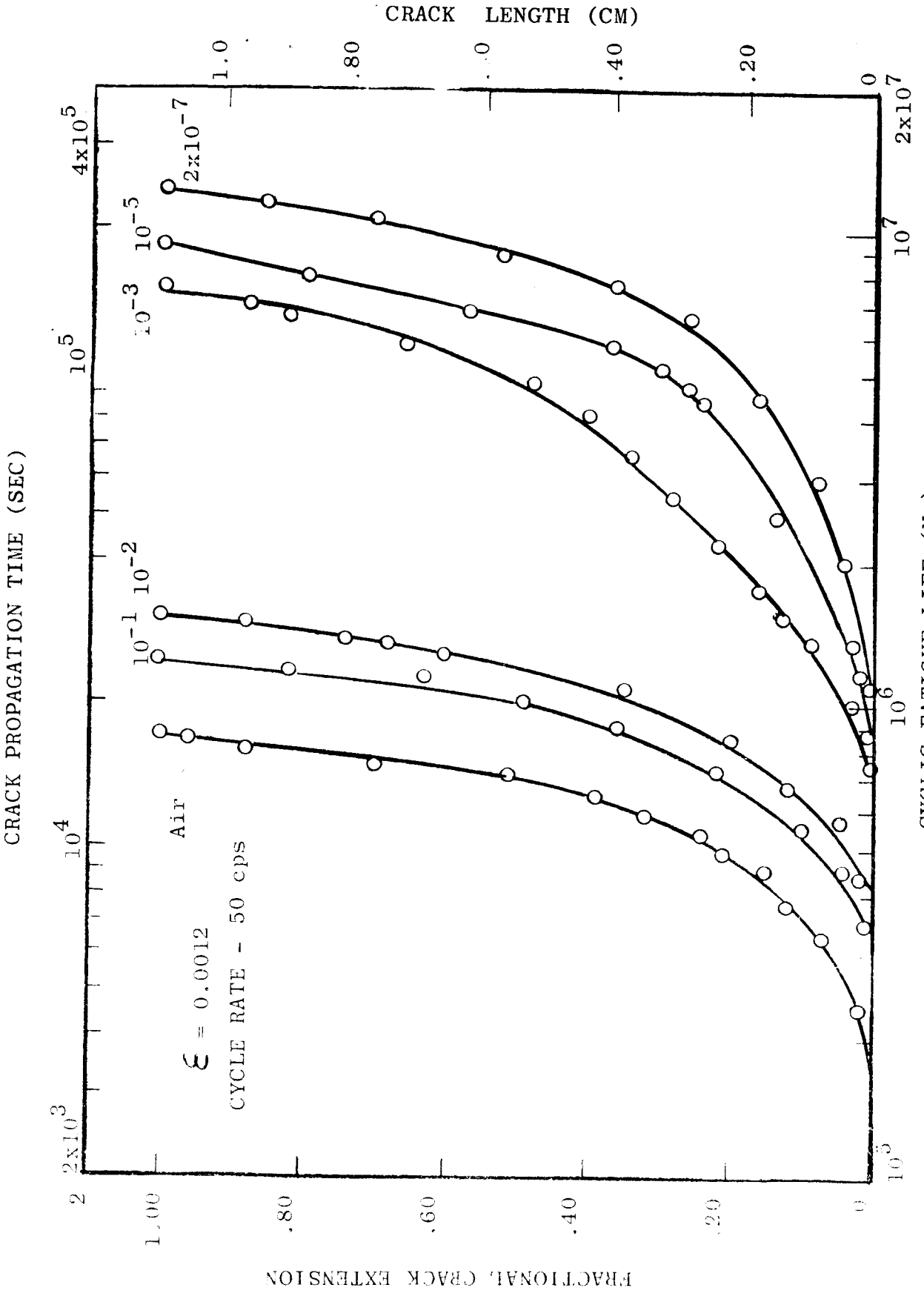

EFFECT OF VACUUM ON THE RATE OF FATIGUE CRACK GROWTH AT CONSTANT STRAIN AMPLITUDE AND BENDING RATE.

shown in the P-N curves, the major increase in crack retardation occurred in the pressure interval between 10^{-2} and 10^{-3} torr.

The effect of plastic strain level on the fatigue crack growth is illustrated in Fig. 12 for the data obtained at 1×10^{-5} torr with a cyclic rate of 50 cps. It is apparent that the vacuum retardation effect increased considerably at the lower stress - strain levels. Fig. 13 indicates the effect of cyclic frequency on crack propagation time as a function of pressure for the series of tests with $\varepsilon = 0.0012$. The time required for unit crack extension at 50 cps was less than at 25 cps, but more than half the 25 cps values, indicating that the fatigue resistance increased with cycle frequency.

Measurements of the initial crack growth rate in cm/cycle were obtained from the slopes of the crack propagation curves. Fig. 14 illustrates the data obtained in air, 10^{-3} and at 2×10^{-7} torr as a function of plastic strain amplitude and cycle rate in the range 0 - 10 pct crack extension. It is evident that the vacuum environment substantially retarded the growth rate at all strain levels. At pressure levels below 10^{-3} torr, the fatigue tests run at the higher reverse bending rate (50 cps) showed a uniform decrease in the rate of crack extension per cycle compared to the tests run at 25 cps. The slower propagation rate may be attributed to the greater extension per unit time at the higher cyclic rate, enabling the crack to progress faster than the rate of gas adsorption to contaminate the newly created crack surfaces.

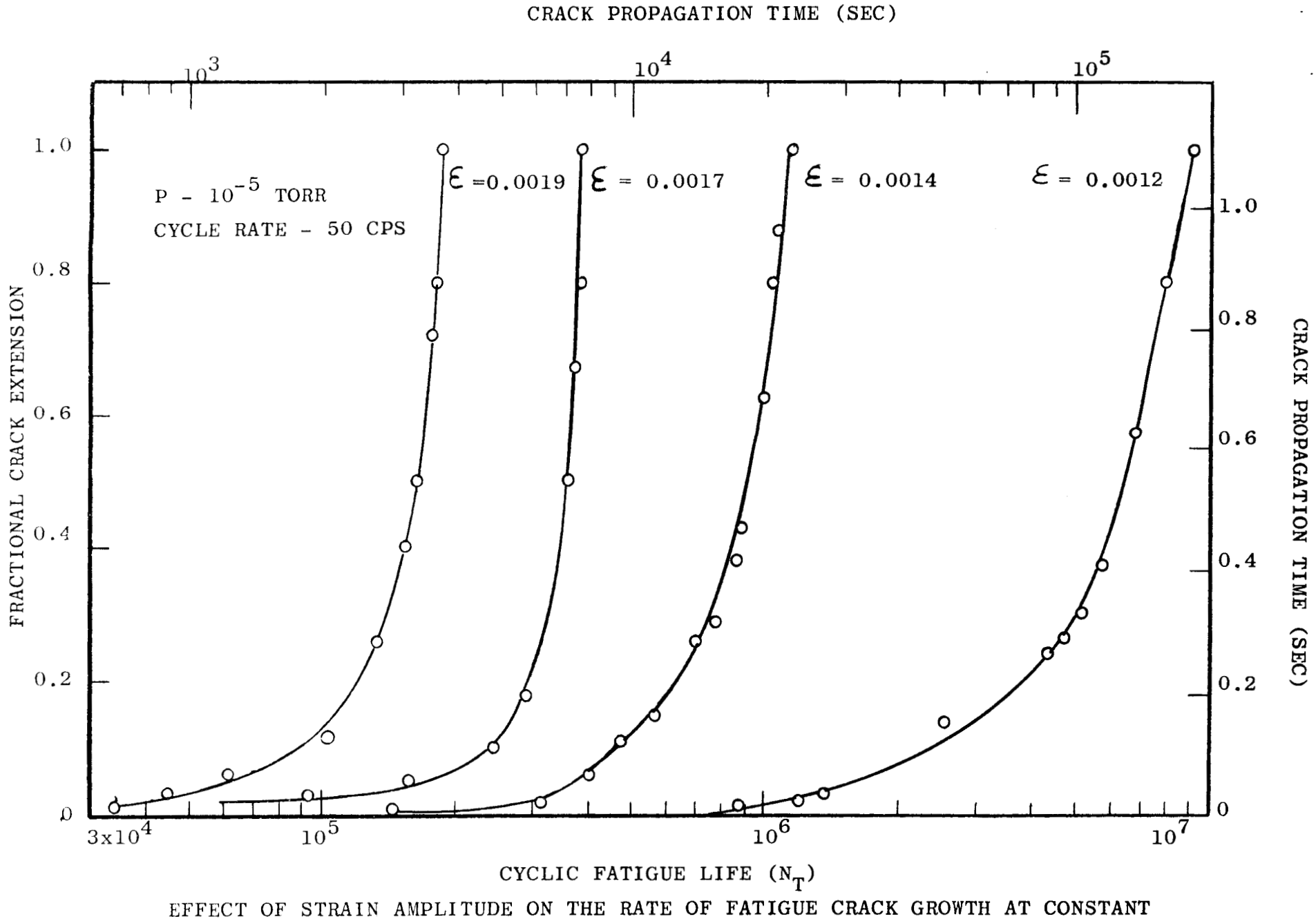

EFFECT OF STRAIN AMPLITUDE ON THE RATE OF FATIGUE CRACK GROWTH AT CONSTANT PRESSURE AND CYCLIC FREQUENCY.

FIGURE 12

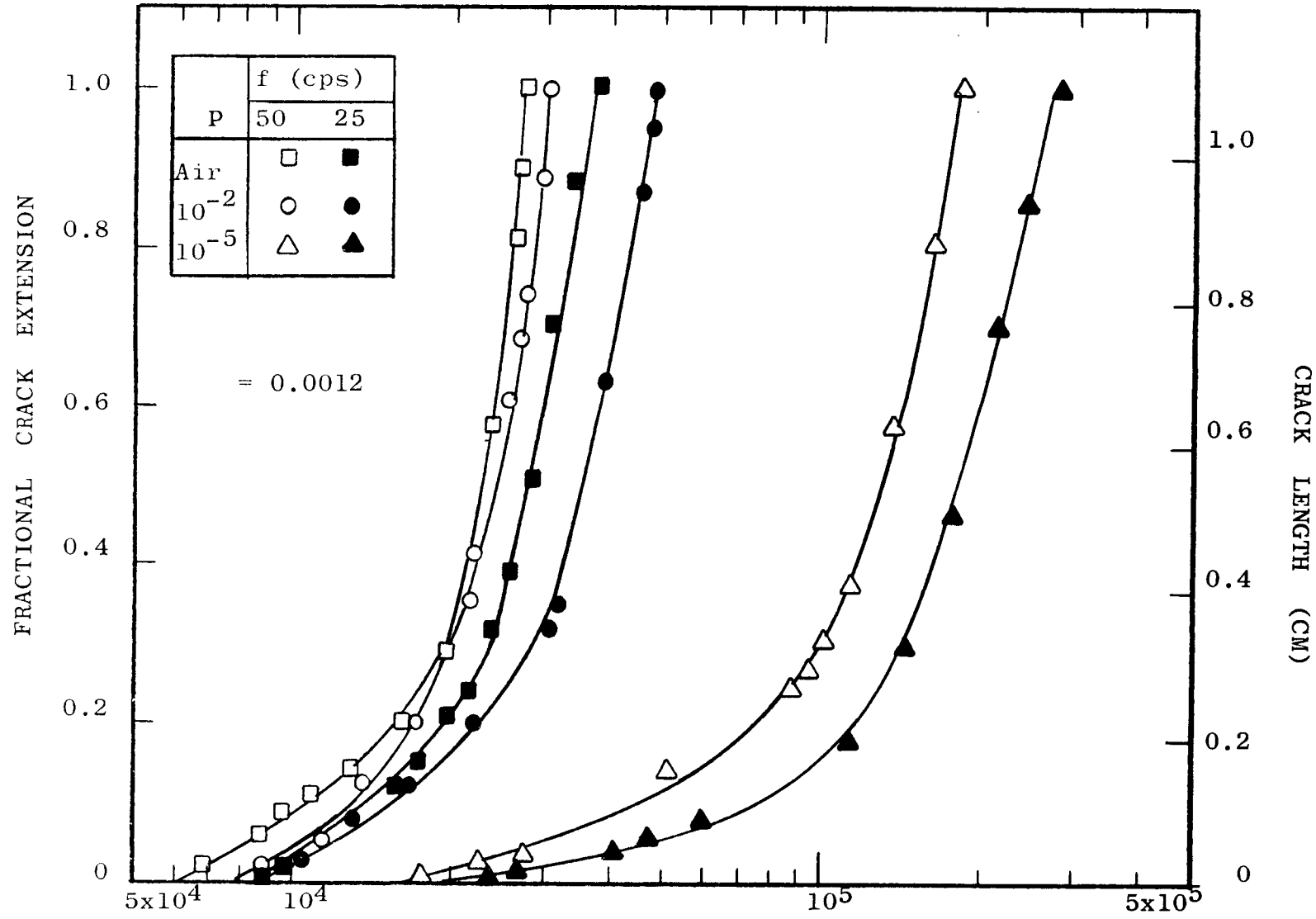

EFFECT OF CYCLIC FREQUENCY ON THE RATE OF FATIGUE CRACK GROWTH AT VARIOUS VACUUM LEVELS.

FIGURE 13

FIGURE 14

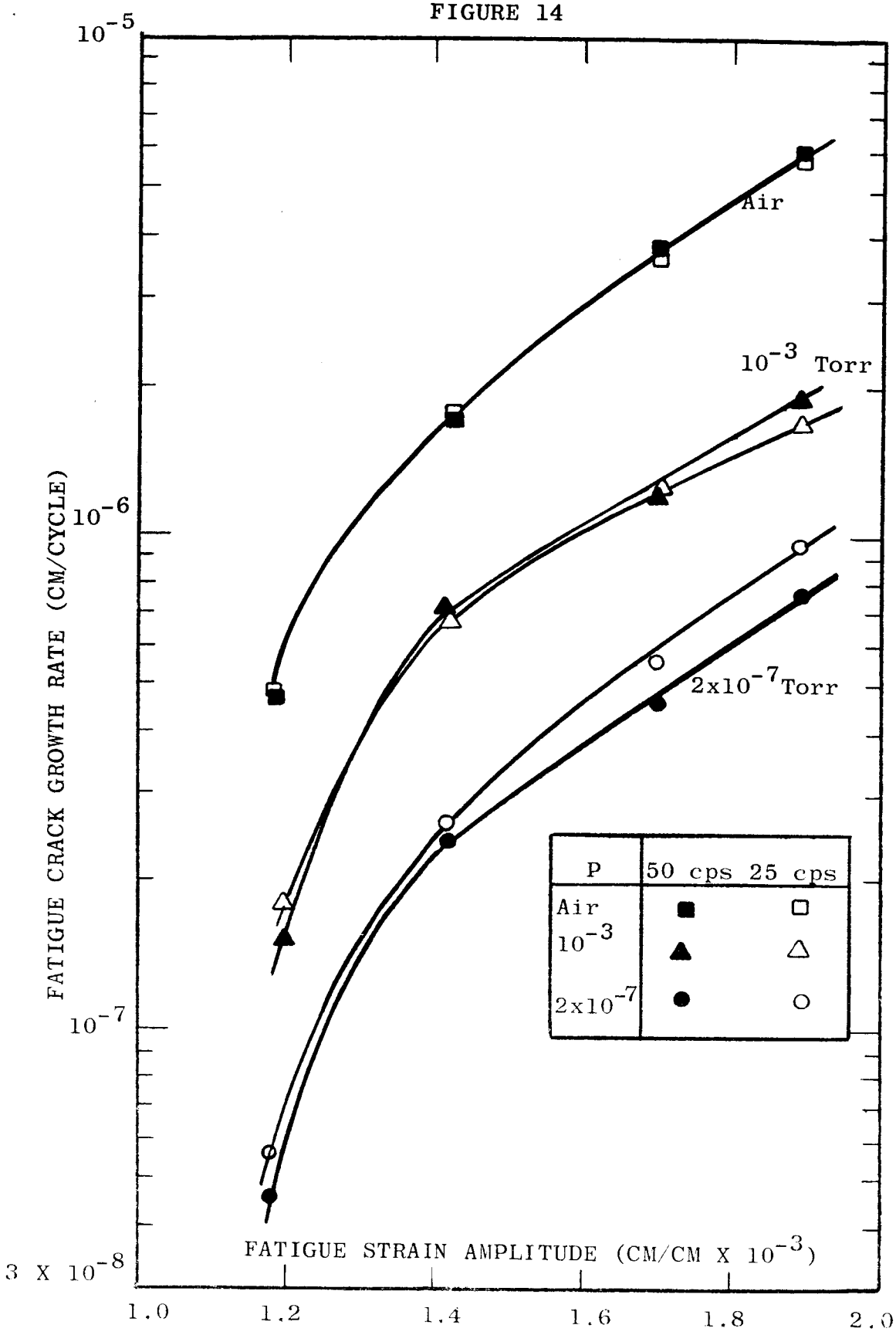

VARIATION OF THE FATIGUE CRACK GROWTH RATE WITH PRESSURE, STRAIN AMPLITUDE AND CYCLIC FREQUENCY

Fatigue Stress-Strain Measurements

In the course of the fatigue experiments, selected specimens were monitored for the moment force required for maximum deflection as a function of fatigue life. The cantilever moment force was measured using a four resistance strain gauge bridge cemented to each of four of the specimen base supports. The bridge recorded the deflection of the base upon application of the drive force to the cantilever-beam specimen. The recorder strain was calibrated with fixed weights attached to the specimen, so that the deflection could be interpreted in terms of a moment force.

A representative force vs. cyclic life curve is shown in Fig. 15 for aluminum in air. It is apparent that the moment force changed very little throughout the major portion of the fracture life, although a small amount of strain softening, shown as a decrease in the recorder amplitude, was detected during the first 10,000 cycles. However, after 50,000 cycles, corresponding to the formation of the major crack, the moment force began to dropp off sharply. After 90,000 cycles or 25 pct extension of the crack, the force decreased to zero indicating that the crack had penetrated through the outer stress elements to the center of the specimen. The strain recorder response may be compared to the rate of crack extension as determined optically.

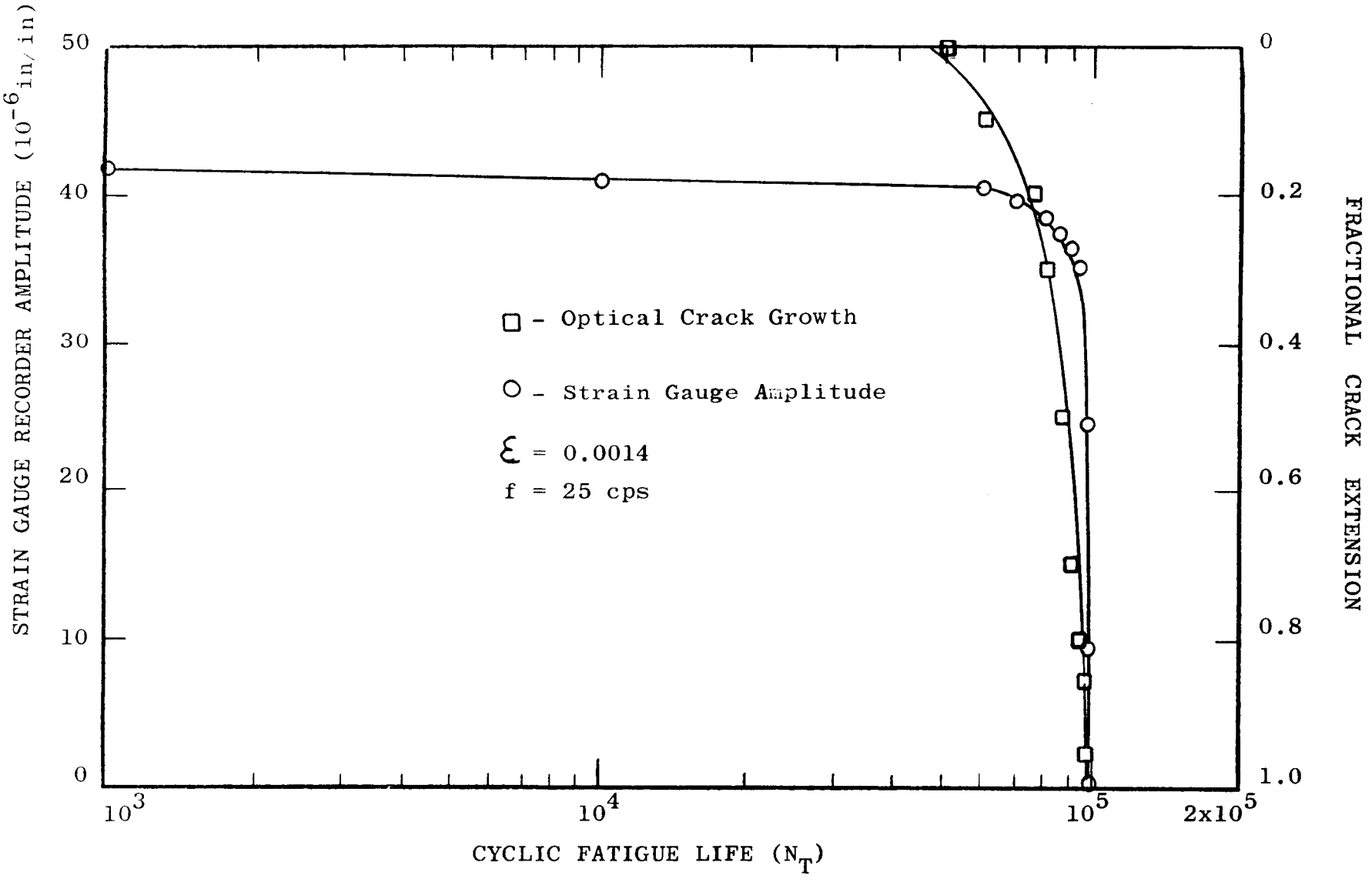

COMPARISON OF OPTICAL AND STRAIN GAUGE MEASUREMENTS OF CRACK EXTENSION AND MOMENT FORCE, RESPECTIVELY, FOR THE FATIGUE OF ALUMINUM IN AIR.

FIGURE 15

Similar curves were obtained in vacuum with negligible strain softening obtained in the crack initiation phase of the fracture life. The small change in force with fatigue loading may be attributed to the pre-hardened condition of the 1100 - H14 aluminum samples.

3.5 DISCUSSION

The effect of the surface vacuum environment in sharply increasing the fatigue resistance has been attributed generally to the removal of oxygen from the vicinity of the fatigue crack. [10] The proposed mechanism is the dissociation and adsorption of oxygen molecules on the freshly formed crack surfaces to form the metal oxide, thus inhibiting the reversal of slip along the fatigue glide bands and preventing rewelding of the cracks.

In the case of aluminum, a second mechanism comprising of dissociation of water vapor molecules and subsequent adsorption of hydrogen (H^+) ions on the crack surfaces has been advanced in order to explain the accelerated effect of water vapor in the atmosphere in promotion crack formation and growth. [5] Since aluminum is a reactive metal, it is likely that both mechanisms may operate during fatigue stressing.

The data presented in the present work cannot clearly distinguish the controlling mechanism. However, both processes must account for the well defined transition pressure ($\sim 10^{-2}$ torr) below which the crack propagation was substantially retarded.

The effect of a reactive gaseous environment on crack growth may be attributed to the kinetics of molecular transport from the outer surface to the root of the advancing crack.[11] Assuming that the desorption rate at the newly created crack surfaces is negligible, the arrival rate of molecules at the crack base may be expressed as:

$$R_a = \frac{3.5 \times 10^{22} \; P \; A}{G \; (MT)^{1/2}} \qquad (2)$$

where P is the partial pressure of the gas in mm Hg, A is the cross-sectional area of the gas molecule, M is the molecular weight, T is absolute temperature and G is a geometrical factor expressing the crack configuration.

Alternatively, Eq. (2) may be expressed as the time required to adsorb a monolayer of adatoms on to the fresh metal surface per unit surface area:

$$t = \frac{G \; (MT)^{1/2}}{3.5 \times 10^{22} \; PA} \qquad (3)$$

For the usual fatigue crack configuration, G may be approximated as $G \sim 3/8 \; l^2 / r^2$ where l is the crack depth and r is the average width of the narrow slit.

Eq. (3) may be used to estimate the rate of gas adsorption down the fatigue crack for comparison with the measured crack growth rates obtained as a function of pressure. Assuming that the crack advances into the specimen depth (half-depth = 0.24 cm) at the same

rate as it propagates across the gauge section surface, we may calculate the time required to adsorb a monolayer of oxygen or water vapor after 10 pct of the crack extension for comparison with the measured times for the initial 10 pct of the fatigue crack extension. Taking the values: $l = 0.024$ cm, $r \sim 10^{-5}$ cm, $T = 300°K$, $M = 32$ for O_2 and 18 for H_2O and $A = 1.0 \times 10^{-15}$ cm^2 for O_2 and 1.7×10^{-15} cm^2 for H_2O, respectively, the following expressions can be derived:

$$t_{O_2} \simeq 6.1/P \text{ sec.} \qquad (4)$$

$$t_{H_2O} \simeq 2.7/P \text{ sec.}$$

The theoretical crack adsorption times given in Eq. (4) are plotted in Fig. 16 as a function of pressure. The actual fatigue crack growth rates for $\varepsilon = 0.0012$ for aluminum at 25 and 50 cps are presented for comparison. It is evident that at pressure levels above 10^{-3} torr, the growth rate was faster than the adsorption rate. Thus, the transition pressure 10^{-2} - 10^{-3} torr observed in Fig. 8 can be tentatively accounted for by the kinetics of molecular adsorption.

It may be noted from Fig. 16, that increases in the crack propagation rate (decrease in propagation time) due to increased fatigue stress or cycle frequency can raise the transition pressure to the atmospheric level, thus eliminating the vacuum enhancement of fatigue resistance. The small vacuum effects noted in static tensile deformation may be attributed to this cause. In the same way, lowering the adsorption rate (eg. a non-reactive metal such as gold) will have a similar effect.

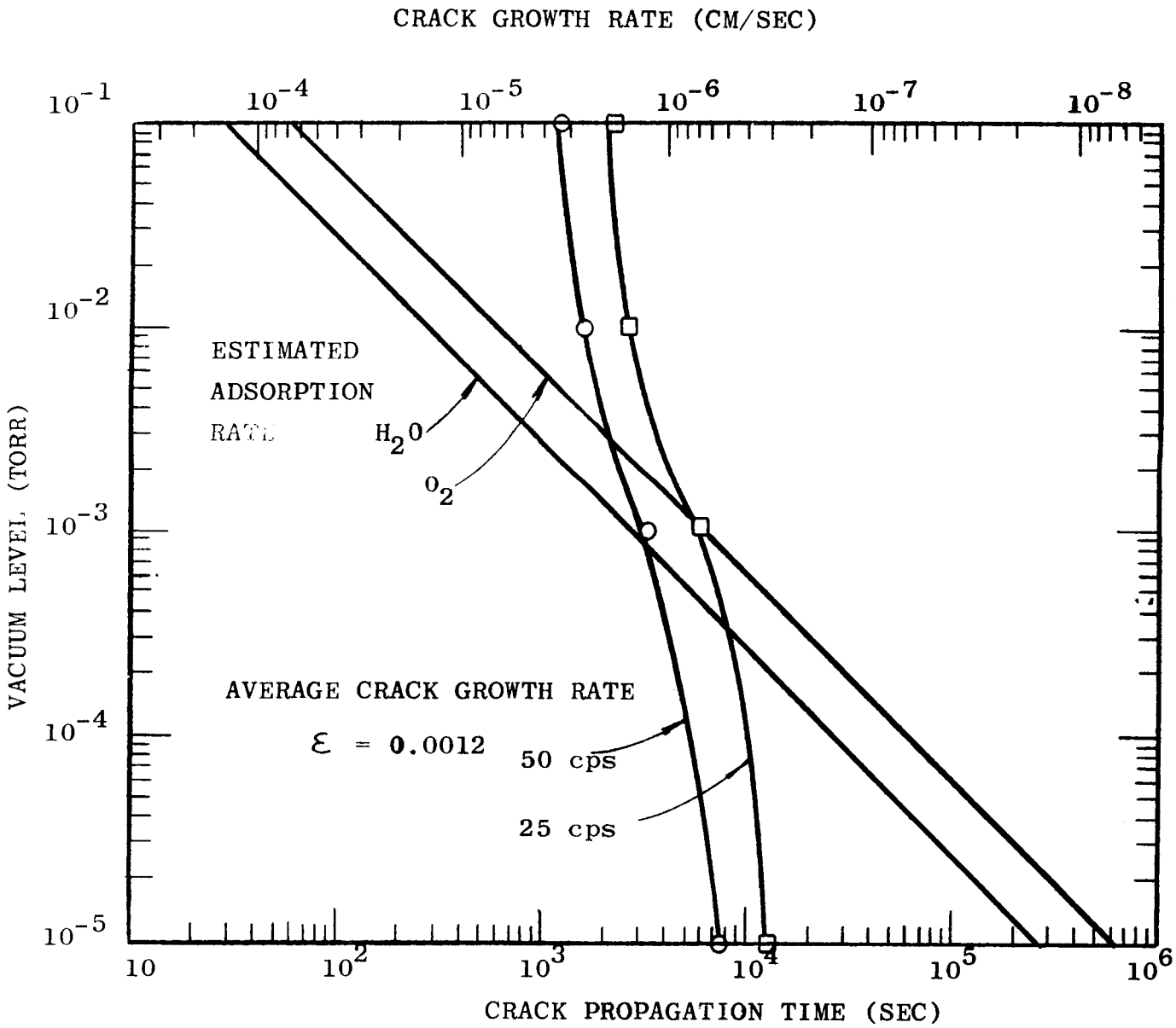

COMPARISON OF FATIGUE CRACK GROWTH RATE AND GAS ADSORPTION RATE

FIGURE 16

4.0 PHASE II

4.1 Introduction

In order to examine the fatigue behavior of aluminum at extremely low pressures simulating the space environment, it was decided to design and construct a fatigue testing apparatus to be incorporated into the Extreme High Vacuum (XHV) facility developed at National Research Corporation. The XHV system, with an effective working chamber of about 4 cubic feet, can reproducibly provide vacuum levels down to 10^{-13} torr.

After consideration of several widely differing design concepts for an XHV fatigue device, it was decided to utilize a sealed electromagnetic vibration exciter to drive a number of specimens mounted concentrically to a cantilever base. The entire fatigue unit was conceived to be placed inside the XHV vacuum system in order to minimize the severe mechanical, thermal and vacuum design constrictions. In turn, however, this concept necessitated careful design of a novel bellows seal assembly to transfer the driving force from the sealed exciter at unit atmosphere inside the vacuum chamber to the specimens.

4.2 Basic Design Considerations

Stress and Materials

The existing XHV apparatus, shown schematically in Fig. 17, generates pressures as low as 10^{-13} torr by means of a liquid helium cooled jacket around the working volume. In order to minimize thermal leakage, mechanical and electrical connections must be

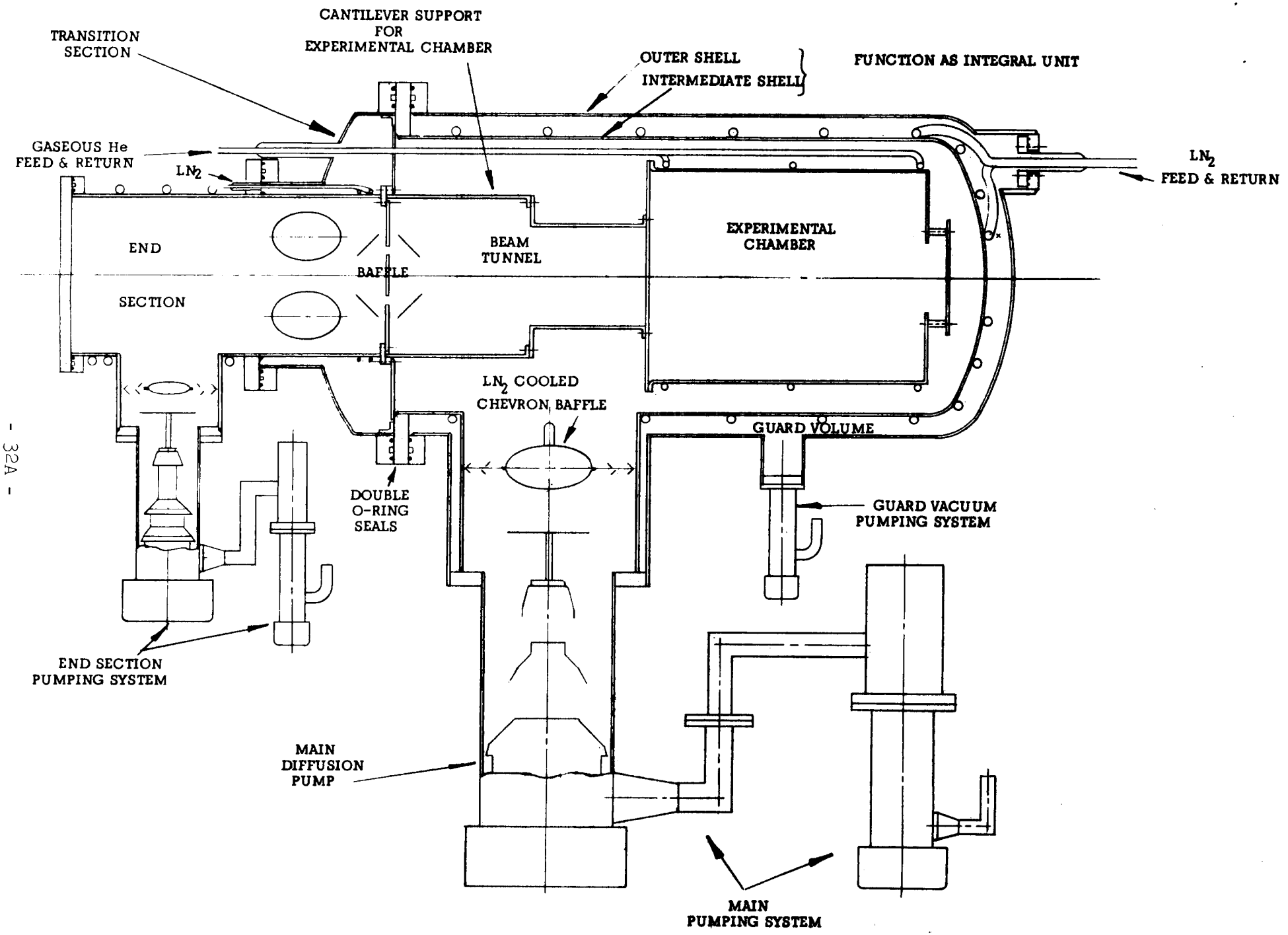

FIGURE 17 - EXTREME HIGH VACUUM CHAMBER

fed through secondary guard vacuums over a distance of up to six feet. In view of this, a mechanical power source to provide rapid alternating motion up to 200 cps positioned over 6 feet from the specimens was deemed impracticable. A survey of compact power sources capable of being positioned inside the vacuum system led to the choice of an electromagnetic vibrator capable of providing up to 50 lbs. thrust through an amplitude of $\pm$ 0.10 in. at frequencies up to 200 cps. Within these limitations, calculations were made to determine the size, stroke, and number of specimens which could be tested at one time. Aluminum types 1100 and 7075, 6 Al - 4V - titanium alloy and AM 350 steel were investigated. It quickly became apparent that materials such as AM 350 required considerably more energy than aluminum to fracture in fatigue. The specimen size was, therefore, reduced to what was considered a practical, economical minimum size while maintaining the same proportions and shape as the specimens used in Phase I. The nominal two inch stress length was reduced to one inch.

The number of specimens which could be fatigued at various amplitudes and frequencies was derived as follows:

Assuming:

50 lbs. total available magnetic force, 20 to 200 cps

Shaft and shaker moving mass (m) = 0.75 lb.

Spring rate of bellows seal = 100 lb/in.

Spring rate of strain gauge springs = 20 lb./in.

Spring rate of vibrator spiders = 30 lb./in.

Let y = single amplitude, inches; f = frequency, cps

Then the inertia force = $my(2\pi f)^2 = \frac{0.75}{386} \; y \; (2\pi f)^2$, or

$$F = 0.0766 \; (y \; f^2) \text{ lbs.} \tag{5}$$

The net available force to deflect specimens is:

$$F_{net} = 50 - 150 \; y - 0.0766 \; y \; f^2 \text{ lbs.} \tag{6}$$

The results are plotted in Fig. 18.

The number of specimens which can be fatigued to fracture with the energy available from the exciter depends on the amplitude at which the specimens are run. The formula used below is derived from a derivation given in Timoshenko and McCullough[12]:

$$F = \frac{b \; h^3 \; E \; y}{6 \; u^3} \tag{7}$$

where: b = width of base of specimen, inches

h = thickness of specimen, inches

E = Young's modulus for the specimen material, psi.

y = Deflection of specimen, inches

u = length of specimen, inches

For aluminum type 1100-H14:

E = 1 x 10^7 psi; take h = 0.060 inches. Then, $\frac{F}{y} = \frac{b \; h^3 \; E}{6 \; u^3}$ = 90.0 lb/in per specimen.

For eight specimens, the spring rate = 8 x 90 = 720 lb/in. This is shown on Fig. 18 as a dashed straight line.

The specimen stress which corresponds to these deflections is calculated as follows:

$$S = \frac{h\ E\ y}{u^2} \qquad (8)$$

where S = bending stress, psi and the other symbols are as shown above.

For the specimen configuration selected; h = 0.060 in, u = 1.0 in. and $S = 60 \times 10^{-3}$ y. The corresponding maximum bend stress vs. deflection is shown in Fig. 19.

As shown in Fig. 18, it is evident that for an amplitude of 0.035 inches, a force of 25 pounds is required to deflect the specimens as shown on the spring rate curve for 8 specimens each 0.060 inches thick. Fig. 18 shows that at 100 cps and .035 inches deflection, 34 pounds are available from the exciter. Therefore, 8 aluminum specimens can be run at somewhat over 100 cps at a stress of 21,000 psi. Similarly at 200 cps, 8 specimens can be run at 12,000 psi sufficient to cause failure in approximately 4×10^6 cycles in vacuum of 10^{-7} torr.

A material such as AM 350 has an elastic modulus approximately 2.9 times higher than aluminum. The vibrator could drive 8 specimens to a stress of approximately 40,000 psi at 20 cps. This is well below the endurance stress of AM 350. To obtain the higher desired stress, specimens thicker than 0.060 inches will be required. Otherwise, excessively high amplitudes would be required.

Other materials such as titanium with a modulus of approximately 1.5×10^6 psi and a lower endurance limit would come between the

VIBRATING FORCE AVAILABLE (F_{NET})

AND SPECIMEN SPRING LOAD VS.

AMPLITUDE

FIGURE 18

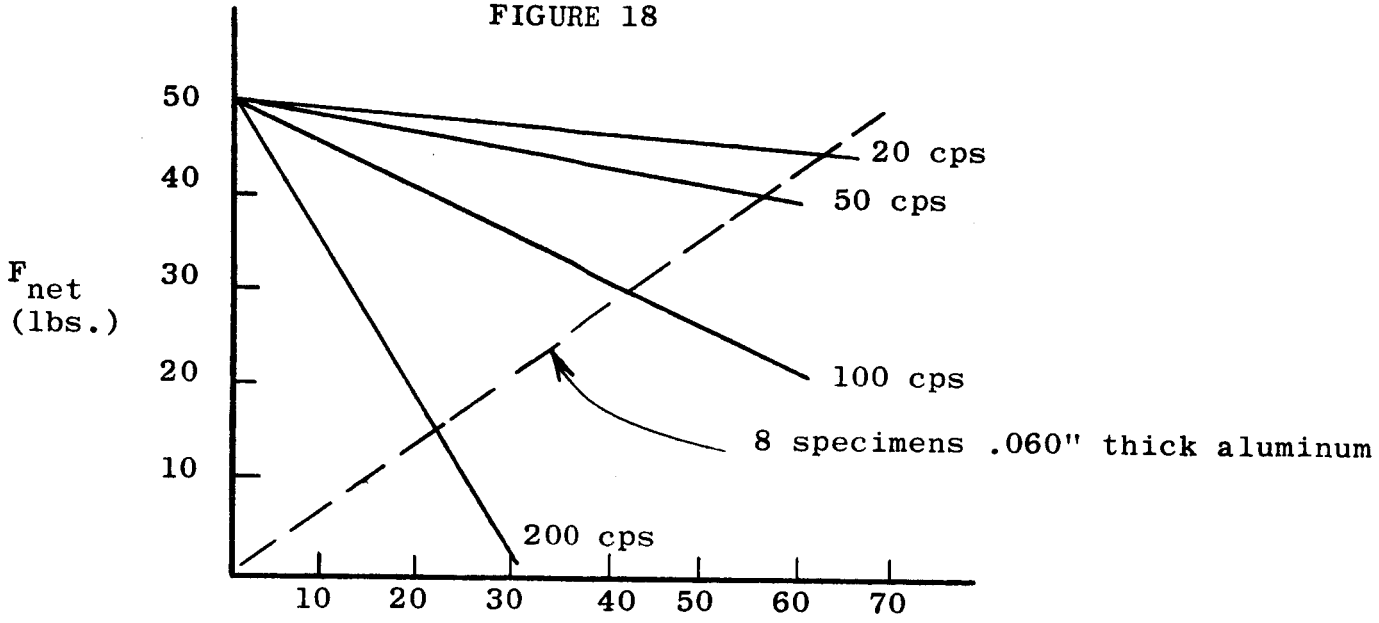

* * * *

FIGURE 19

SPECIMEN BENDING STRESS VS. DEFLECTION

(0.060 Inch Thickness)

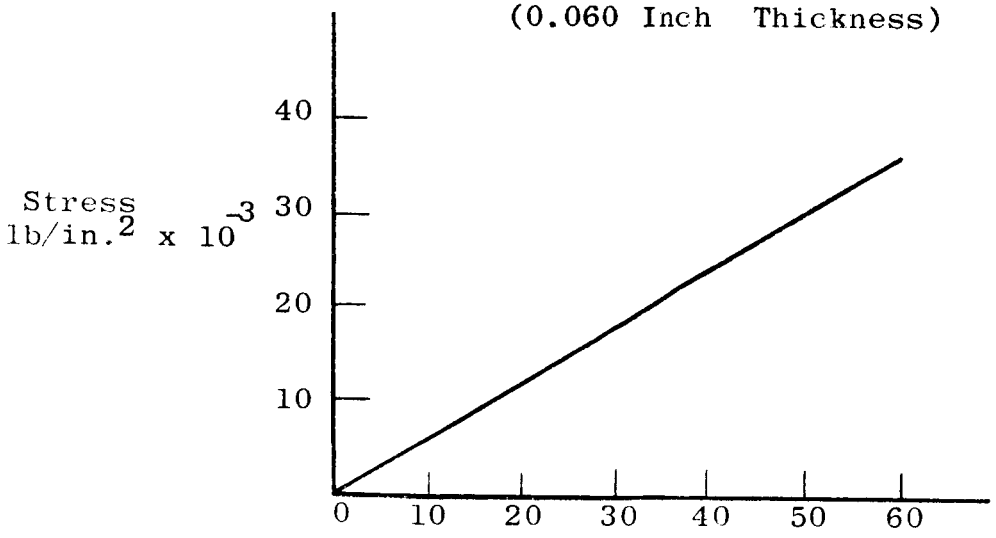

extremes of aluminum and AM 350. Four titanium specimens could be tested at one time at a frequency of approximately 50 cps. Amplitudes and frequencies compatible with the exciter capacity can be determined by drawing the appropriate spring rate for the desired specimens on Fig. 18. Specimens would be slightly thicker than .060 in. for optimum operating amplitude at the required stresses.

Typical material characteristics are shown below for convenience.

TABLE I

MECHANICAL PROPERTIES

Material	Endurance Limit (psi x 10^{-3})	Young's Modulus (psi x 10^{-6})	Test Stress Range (psi x 10^{-3})
Al 1100 H14	7	10.0	12 - 19
Al 7075 T6	10	10.4	18 - 27
Ti 6 - 4	26	14.5 -19	40 - 66
AM 350 CRT	70	29	120 - 190

* * *

Gold "O" Ring Seal Design

National Research Corporation has had successful experience with gold seals using 0.040 inch diameter gold wire rings clamped between flat highly polished surfaces. The design of the gold seal flanges is described below.

The yield strength of the gold was estimated at 30,000 psi. It was assumed that the ring would be compressed to 0.020 inches

thickness. The compression area, therefore, becomes:

$$\frac{\pi}{4} d^2 = (\text{width}) (\text{thickness})$$

width = 0.0628 inches.

The compression force per linear inch of seal = 30,000 x 0.0628 = 1900 lb/inch. Bolts are spaced 0.9 inches apart requiring 1700 lb per bolt.

High strength stainless steel bolts of the standard Pressed Steel Company Unbrako KS812 series were selected to prevent bolt creep at the high temperatures of bakeout of the vacuum system. Bolts 5/16 inch diameter with fine thread were selected for maximum strength. These bolts are rated at approximately 3800 lbs each induced load when torqued to 200 in. - lb. with "no additional lubrication". The bolts can be torqued to 245 in.- lb. With the 1700 lb. load on each bolt, the resulting tensile stress is 32,000 psi. The vendor provided data showing stress relaxation from 65,000 to 55,000 psi after 50 hours at 800°F. Since the temperatures and stresses to which the bolts will be subjected are less than these values, the design is considered conservative and no significant creep should occur.

The shear stress in the 304 stainless steel flange is based on the pitch diameter of the threads and a thread engagement of 1.5 x bolt diameter:

$$S_s = \frac{\text{force}}{\text{shear area}} = 8,900 \text{ lb./in.}^2 \qquad (9)$$

This is well below the creep strength of 304 stainless steel at 750°F and the creep in the flange should be negligible.

The thermal expansion of 304 stainless steel according to handbook data is slightly greater than that for gold. The elongation of the bolts, however, $\frac{S}{E} u = 0.0011$ inches is greater than the difference in expansion between the gold and the 304 stainless steel:

$$u (\alpha_{304} - \alpha_{gold}) \Delta T = 14.0 \times 10^{-6} \text{ inches} \quad (10)$$

where α is the thermal expansion coefficient. Therefore, the seals will remain tight throughout the temperature cycling.

The deflection of flanges between bolts was calculated according to the expression:

$$y_{Max.} = \frac{1}{384} \frac{w u^3}{E I} = 1.5 \times 10^{-6} \text{ inches} \quad (11)$$

where y = deflection in inches, w = load on one bolt in lbs., u = distance between bolts, I = moment of inertia of flange, and E = Young's modulus of flange material. This deflection is several orders of magnitude below the "O" ring compression or the bolt stretch and is, therefore, considered safe.

Electrical Control Circuit Design

A block diagram shown in Fig. 20 outlines the arrangement of electrical components which will be experimentally utilized to develop the control system. The system is intended to provide constant

amplitude even though the spring rate of the specimens changes due to material changes from repeated strains and as the specimens fracture.

The feedback voltage will be provided by strain gauges mounted on spring stock which flexes as the specimens deflect. As shown in Fig. 21, the strain recorded by the gauges is proportional to the specimen deflection given by the expression:

$$\mathcal{E} = 6\left(\frac{u}{2} - x\right) h\, y/u^3 \qquad (12)$$

where u is the spring length, h is the spring thickness, x is a fixed cantilever distance and y is the bend deflection. Taking the design values u = 1.438 in., h = 0.010 in., x = 0.50 in., then $\mathcal{E}$ will be 220. x 10^{-6} in/in. for the maximum deflection y = 0.050 in.

The strain gauges selected have a limitation of approximately 200 micro in./in. for a life of 10^7 cycles according to the vendor. Therefore, the exciter will be limited to amplitudes of less than $\pm$ 0.050 inches in vacuum. This is due to the non-organic ceramic bonding material used on the strain gauge to minimize outgassing. The Sanborn recorder-amplifer has a basic sensitivity of 20 to 50 μ in./in. per cm of scale deflection. With proper gain settings, the Sanborn unit will put out signals from the strain gauges which can be fed through a variable gain control circuit to vary the oscillator amplification. As amplitude changes

BLOCK DIAGRAM OF ELECTRICAL
CONTROL SYSTEM

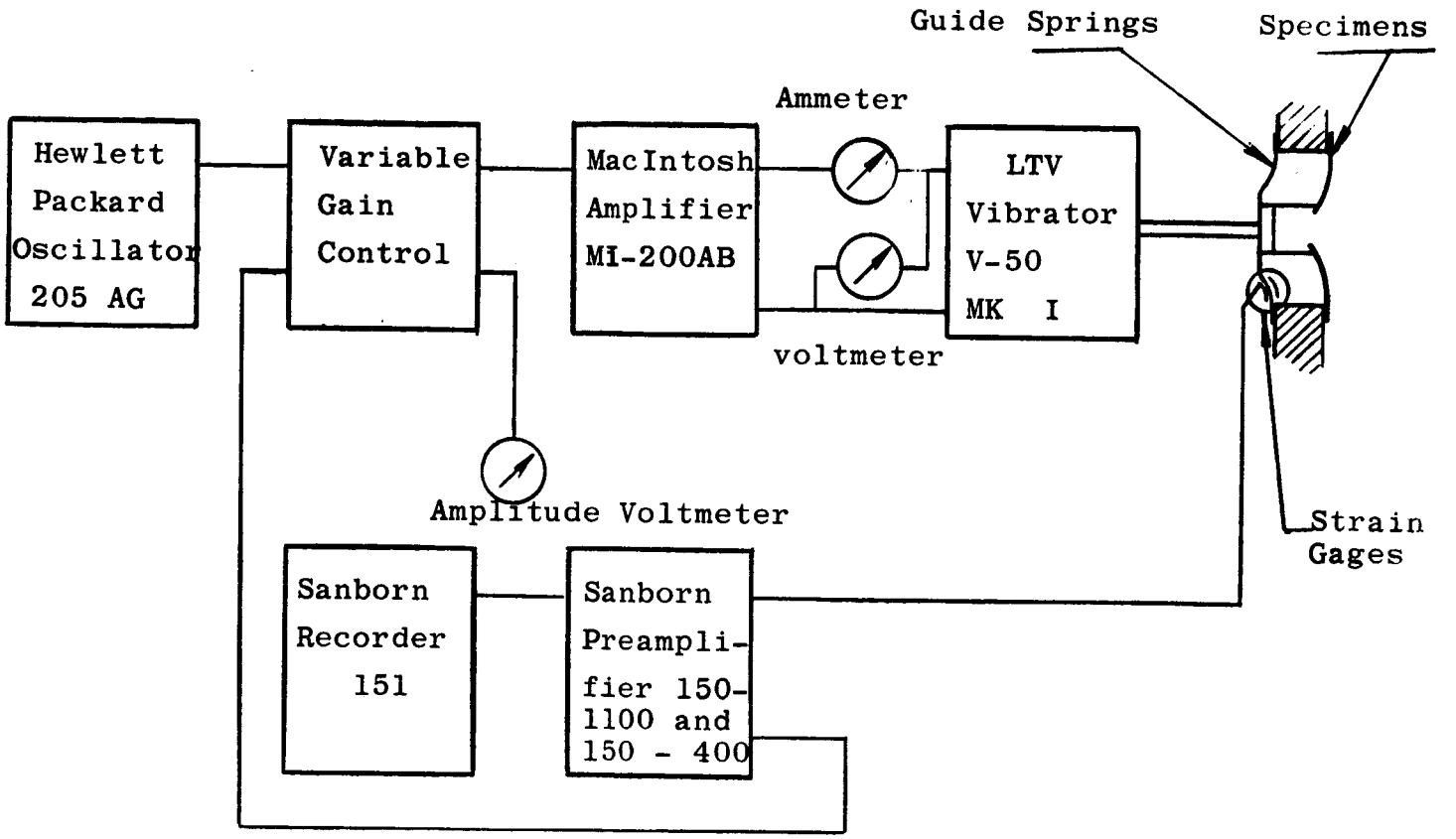

FIGURE 20

***

FIGURE 21

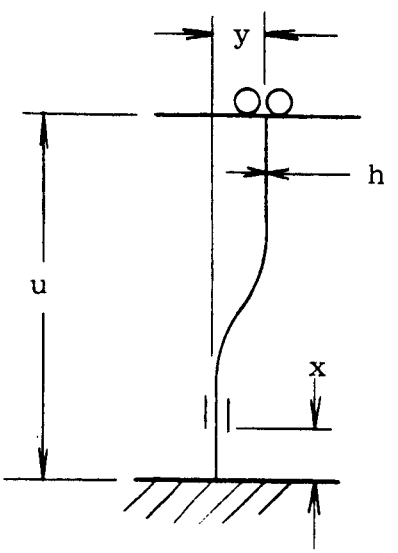

SCHEMATIC OF STRAIN GAUGE MOUNTING SPRING

very slightly due to specimen weakening and breaking, the gain control will hold the specimen amplitude essentially constant.

Vacuum Limitations

It is possible to make some approximations of the level of pressure which the vacuum system will attain. It has been estimated that aluminum with a number 4 finish will have an outgassing rate of 1×10^{-9} torr liters/sec per cm^2 after 4 hours of pumping.[13] For a specimen surface area of approximately 5 cm^2, the gas load from the 8 specimens alone will become 4.0×10^{-8} torr - lit/sec.

The open area of the liquid nitrogen baffle equals 445 cm^2 which provides a maximum pumping speed for air of S = 4900 liters/sec. The system pressure will then be given by:

$$P = \frac{Q}{S} = 8 \times 10^{-12} \text{ torr} \qquad (13)$$

The outgassing rate after 9 hours will drop to about 5×10^{-11} torr liter/sec cm^2. The pressure would then drop to approximately 4×10^{-13} torr. The above estimates are extremely crude, but serve to illustrate that without bakeout of the specimens, the specimens themselves present a gas load to the system which will limit attainable pressures.

4.3 XHV Fatigue Apparatus

General Description

A conceptual schematic shown in Fig. 22 indicates several of the major elements of the horizontal vibrating system within the vacuum environment. The principle difficulty in obtaining really high vacuum while producing mechanical specimen oscillation lies in the means of transferring the energy to the specimen without also introducing a serious gas load to the system. Flexible bellows which expose no organic material to the vacuum are one attractive means of accomplishing this goal.

Another of the difficulties in designing a vibration system is the mechanical coupling between the exciter and the specimens. It would be desirable to locate the vibrator completely externally to the vacuum system and introduce the motion by a relatively long rod or tube. However, the tube must be stiff enough to transmit the force from the exciter to the specimens without lost motion, and the weight of the rod causes a significant energy loss at higher frequencies (above 200 cps). This design is based on a short connecting tube between the exciter and the specimens.

Other features include an air cooled electromechanical vibration exciter enclosed in a vacuum tight container within the vacuum system, slender column type of connecting members between the drive shaft and individual specimens, a liquid nitrogen cooled

SCHEMATIC OF VIBRATOR FATIGUE APPARATUS

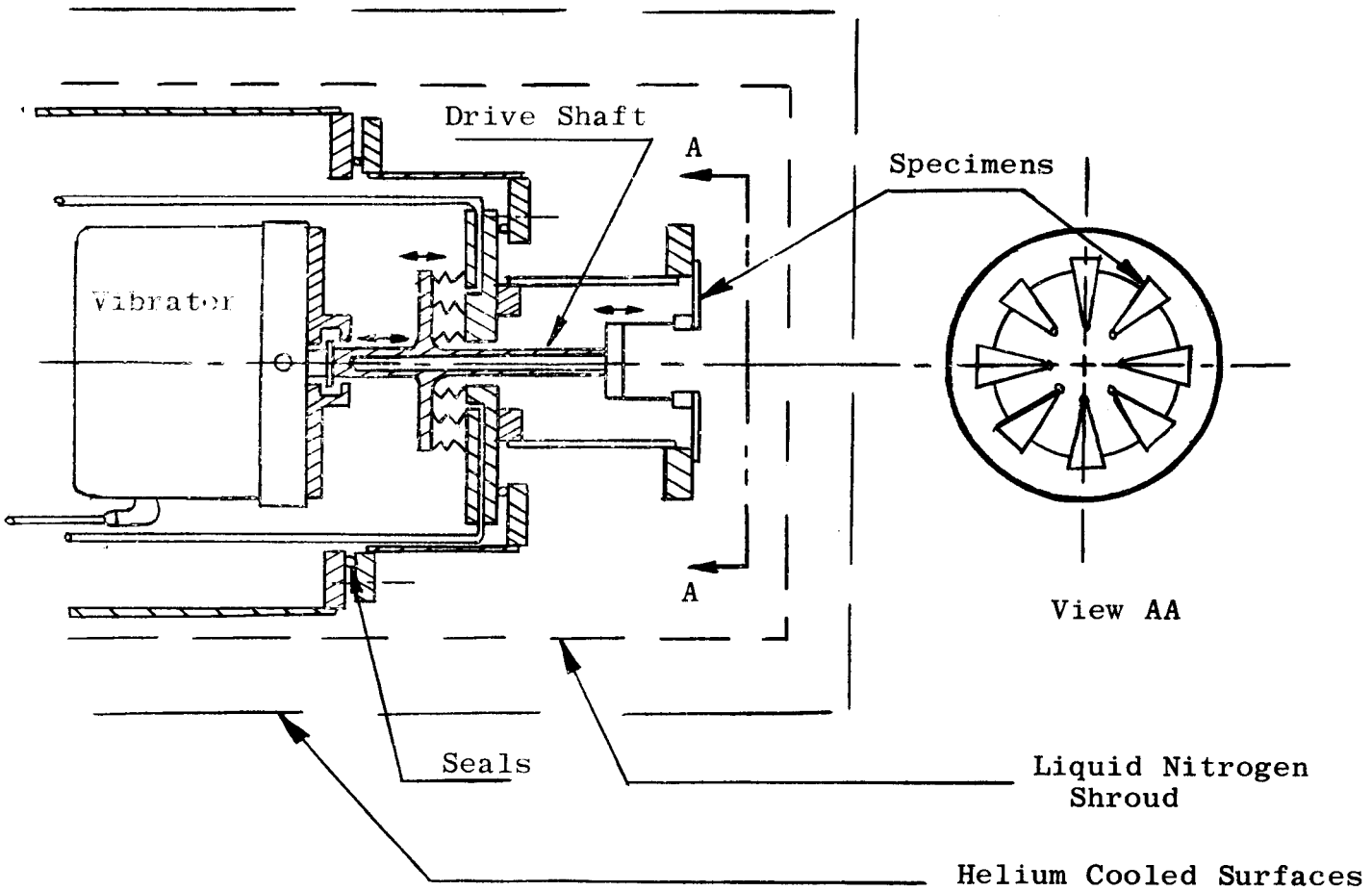

FIGURE 22

shield between the warm room temperature specimens and the helium cooled vacuum system and the necessary thermal control and mechanical supports to complete the system.

Vibrator Exciter

This is a standard electromechanical vibrator generator manufactured by Pye Ling, Ltd. and distributed by LTV Ling Electronics Division. The Model V50 mk 1 has a nominal 50 lb. excitation rating at frequencies between 20 and approximately 100 cycles when it is loaded. It requires air cooling.

Bellows Seal Assembly

The driving shaft extending from the exciter moves horizontally through the bellows seal. The three flexible bellows are concentric as shown in Fig. 22. One end of the bellows moves with the vibrating shaft. The other end is fixed integrally with the vacuum tight enclosure. When the vacuum system is pumped down, there is a differential pressure across the bellows which is compensated by a partial pressure between the outer two bellows and the spring resistance of the bellows. The innermost one allows a vacuum to be maintained on both sides of it. This assures minimum leakage into the vacuum system and provides a safety factor against catastrophic damage if one of the bellows should fail in fatigue. The triple seal also allows the system

A water cooling coil is located around the specimen mounting bracket to allow specimen temperature to be controlled as a variable and during bakeout of the vacuum system.

Specimen Positioner and Shaker Sub-Assembly

During pumpdown of the vacuum system it is necessary to hold the driving shaft in a fixed zero-displacement position to prevent the changing pressure across the bellows from putting excessive strain on the specimens. The specimen positioner is a cylinder assembly concentric with the driving shaft. Its purpose is to accurately position the drive shaft during pumpdown. After bellows pressures have been adjusted, the positioning cylinder is withdrawn beyond the normal range of amplitude.

Within this positioner assembly a mechanical stop is provided to limit the extremes of motion of the exciter which might otherwise be damaged by overdriving.

The entire exciter is mounted in a vacuum tight enclosure sealed with gold "O" rings. Electrical leads, cooling tubes, and control tubes are brought out through a long 1-1/2 inch diameter tube to the end of the system opposite from the specimens. The exciter itself is mounted on a ring which is water cooled and isolated thermally from the vacuum tight enclosures by four studs. The same enclosure is supported on a large horizontal stainless steel

to operate in air with the outer annulus completely evacuated and the inner annulus partially evacuated to compress the bellows to the normal working length.

Specimen Mounting Sub-Assembly

Eight specimens may be arranged radially in a vertical plane (see Figs. 23 and 25) with the smaller ends of the specimens located in line with the driving shaft hub. Since the end of each specimen describes an arc as it deflects from the flat condition, a flexible column is placed between the driving shaft hub and each specimen. This moving hub is centrally positioned by four radial springs in such a way that the fracture of any or all the specimens can put no moment loading back into the exciter.

Strain gauges are attached to two of the radial springs to provide a direct signal to measure and control specimen vibration amplitude. These strain gauges are attached to the springs with Rokide flame sprayed ceramic which presents less gas load to the vacuum system than an organic bond.

The specimen mounting sub-assembly may be loaded with new specimens while on the bench and then it may be placed into the vacuum system and attached to the vibrator with 5 screws. An adjustment on the drive shaft hub allows the specimens to have zero mechanical strain at the same time the electrical signal indicates zero displacement.

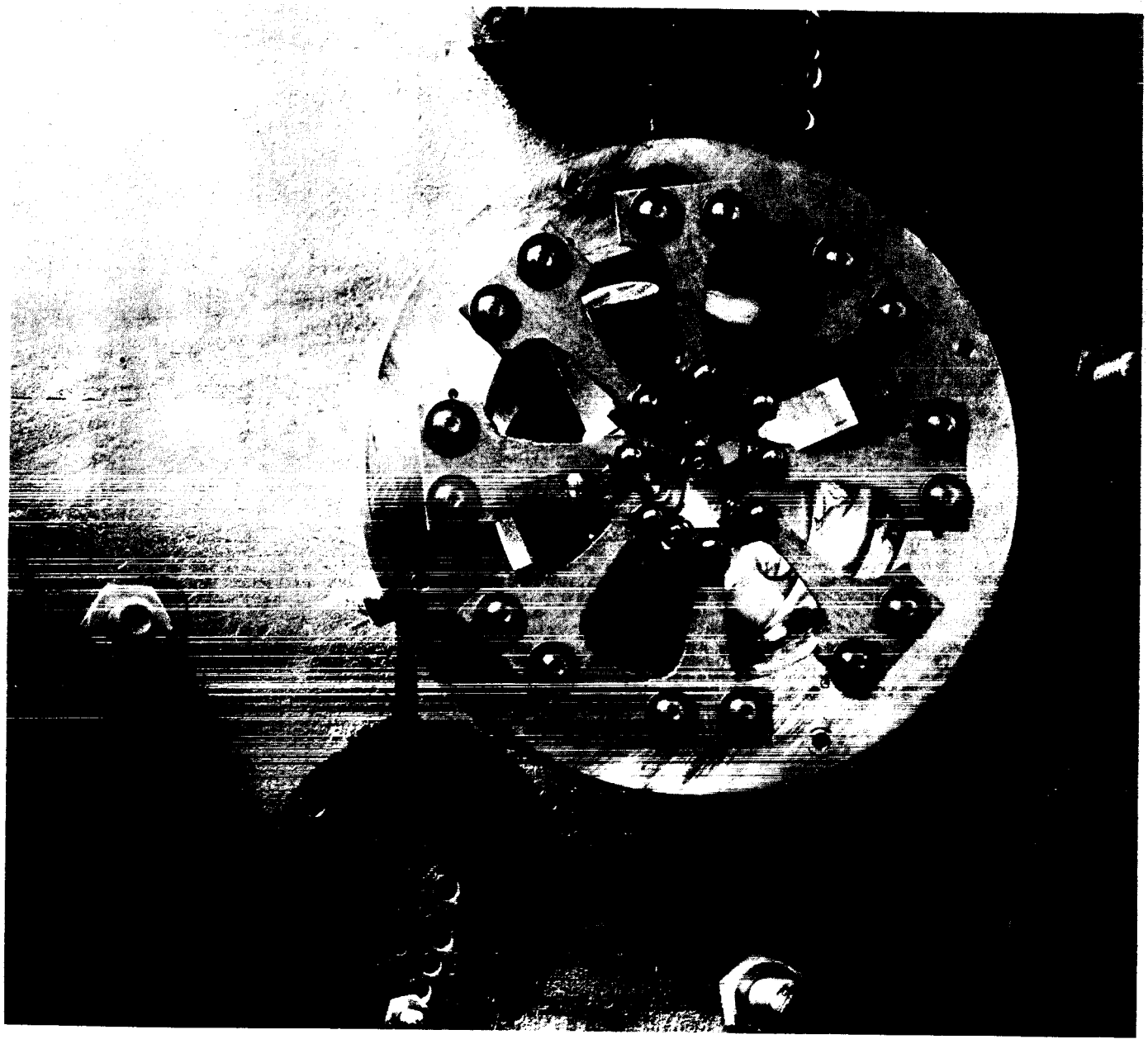

FIGURE 23

Close-up of Dummy Specimens and Push Rods
Strain Gauges Show as White Areas on Support Spring

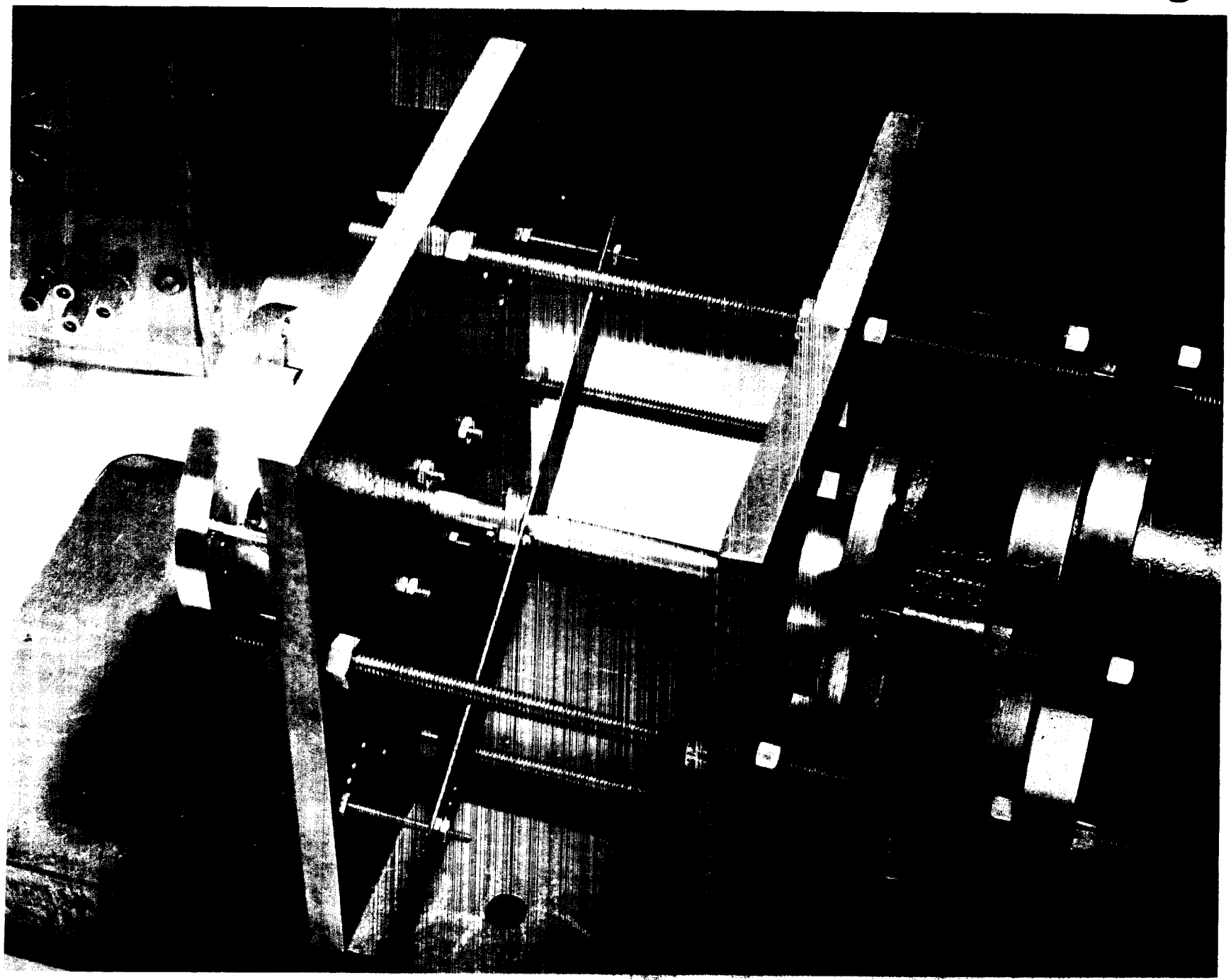

FIGURE 24

Exciter, Push Rod and Flat Spring of Bench Test

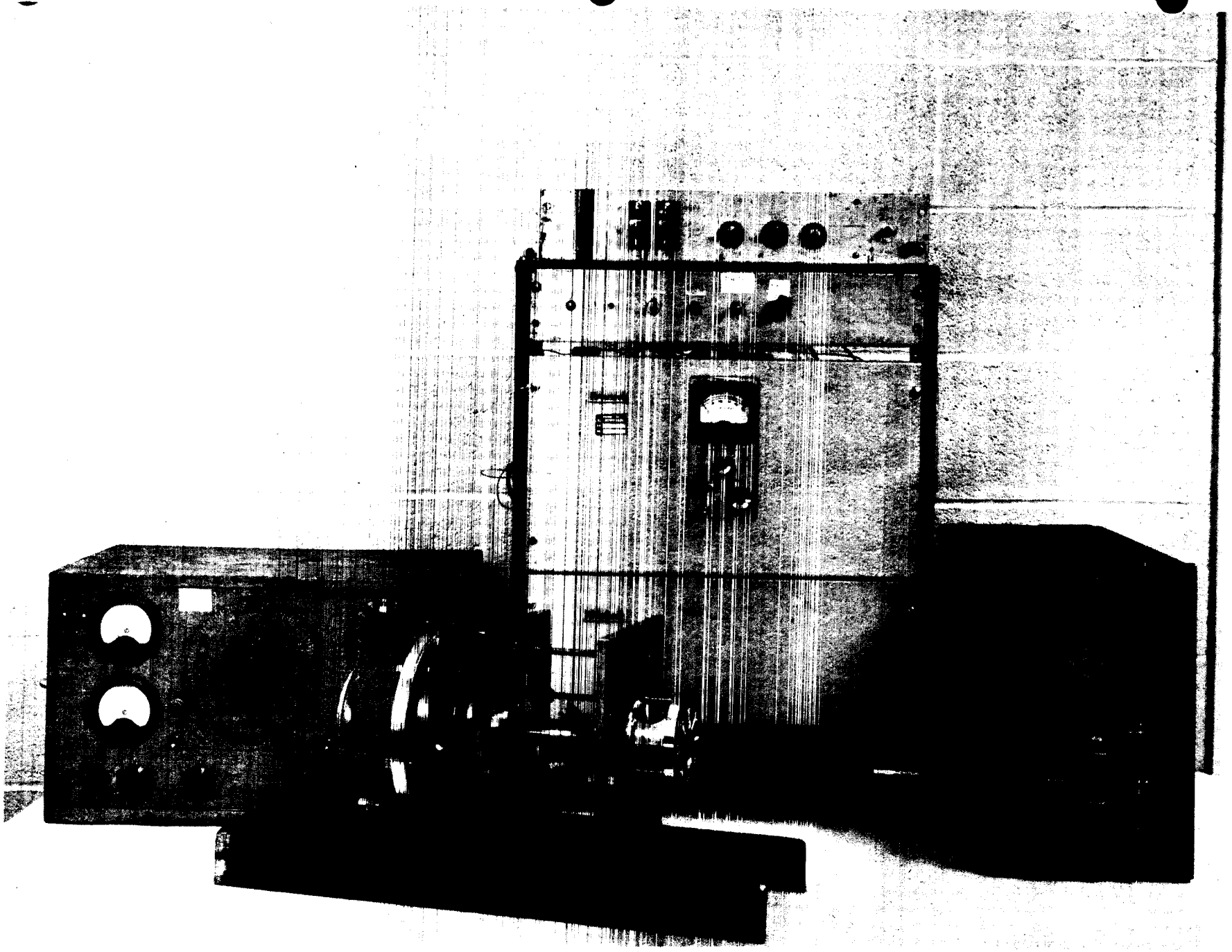

FIGURE 25

Overall View of Exciter Bench Test With Electrical Apparatus

tube which thermally isolates the room temperature enclosure from the liquid nitrogen cooled support surface.

Liquid Nitrogen Cooled Shield

The warm vacuum tight exciter enclosure and the warm specimens would present an excessive heat load to the helium refrigerator system if allowed line-of-sight radiation to the helium cooled surface. Therefore, an optically dense liquid nitrogen shield is provided to surround the entire assembly within the helium cooled cylinder. The nitrogen cooled shield, however, must have passages for the gases not condensed onto the liquid nitrogen cooled surfaces to escape. Hence, a double wall with staggered holes and an end baffle is provided.

The end baffle serves as a support for the cold cathode magnetron gauge whose opening will be directed into the volume of the specimens. In this way the vacuum reading will indicate most accurately the specimen environment.

4.4 Experimental Tests

The earliest experimental work in Phase II of this contract was done with the electromagnetic vibrator exciter to determine its performance. It performed according to vendor specifications in the range of frequencies tested.

A bench test assembly was built to simulate the dynamic characteristics of the actual XHV test device so that the electrical

control system could be developed and tested. Having the unit accessible in air will expedite the assembly and allow direct observation during tests. This development and test work is essentially complete.

Fig. 23 shows 8 dummy specimens on the mounting bracket. The flexible push rods extend back from the small ends of the specimens. The four radially arranged guide springs are visible in the background with white strain gauge areas showing on two of them.

In Fig. 24 shows the flat spring across the drive shaft. This spring simulates the spring effect of the bellows assembly which will be used in the actual vacuum unit.

An overall view of the major electronic instruments and the bench test unit is shown in Fig. 25. Air and water connections will be added later.

Strain gages will provide a signal for specimen amplitude measurement and control. The components and circuits shown in Fig. 20 have been designed, constructed and tested. Control settings will be determined for various operating conditions. The amplitude stability will be measured at several frequencies, and amplitudes.

Later when the vacuum system components have been constructed additional test will be required. One such test will be made to check the performance of the gold seals in the vacuum tight exciter enclosure. The enclosure will be placed in the vacuum system and baked to ascertain what bolt loading is actually required to keep the vessel tight during these temperature excursions.

5.0 FUTURE WORK

It is planned to extend the investigation covered in this report to include the effects of temperature and residual gas content in order to determine the mechanism of atmospheric gas embrittlement on fatigue resistance. The following additional tests have been scheduled:

1. Measurements of the vacuum effect on fatigue of 1100 - H14 aluminum at + 100°C and - 50°C.

2. Determination of the P-N curve for aluminum with pure oxygen and water vapor residual gas environments.

3. Interrupted fatigue tests to determine the effect of vacuum on the crack nucleation and propagation stages of fracture.

4. Extension of vacuum testing to additional materials including age hardened aluminum 7075-T6, 17-4PH stainless steel and 6Al-4V - titanium alloys.

5. Extension of P-N curve data to extremely low pressures using the XHV (Extreme High Vacuum)facility.

REFERENCES

1. M. J. Hordon and L. R. Allen, "Adhesion and Fatigue Properties of Materials in Vacuum", Sixth Annual Symposium On Space Environmental Simulation, St. Louis, Missouri, May, 1965.
2. R. Jastrow, "Lunar and Terrestrial Atmospheres", Advances In Aero Science, Vol. 5, Plenum Press, Inc., New York (1960).
3. H. S. Gough and D. G. Sopwith, Journal of The Institute of Metals (London), Vol. 49, Page 93 (1932).
4. N. J. Wadsworth, "The Effect of Environment On Metal Fatigue", Internal Stresses and Fatigue In Metals, (Ed G. M. Rassiviler and W. L. Grube, Elsevier, Amsterdam), Page 385 (1959).
5. T. Broom and A. Nicholson, Journal of the Institute of Metals, (London), Vol. 89, Page 183 (1961).
6. N. J. Wadsworth, Philosophical Magazine, Vol. 6, Page 397, (1961).
7. K. U. Snowden, Acta Metallurgica, Vol. 12, Page 295, (1964).
8. J. L. Ham and G. S. Reichenback, "Fatigue Testing Of Aluminum In Vacuum", Symposium on Materials For Aircraft, Missiles and Space Vehicles, Special Technical Publication No. 345, ASTM (1962).
9. J. R. Low, Jr., "Microstructural Aspects of Fracture", Fracture of Solids, (Ed D. C. Drucker and J. J. Gilman, Interscience Publications, New York), Page 197, (1963).
10. N. J. Wadsworth and J. Hutchings, Philosophical Magazine, Vol. 3, Page 1154, (1958).

11. K. U. Snowden, Journal of Applied Physics, Vol 34, Page 3150, (1963).

12. S. Timoshenko, and G. H. MacCullough, Elements of Strength of Materials, D. Van Nostrand Company Page 181, 1940.

13. M. Schrank, F. Benner, D. Das, Theoretical and Experimental Study To Determine Outgassing Characteristics Of Various Materials, AEDC-TDR 64-53.